Nuclear Magnetic Resonance

for the People

November 23, 2009

Contents

1.1 Overview

Since NMR was first demonstrated in condensed matter in 1945, the technique has experienced tremendous growth. NMR was commercialized in the 1960's and by the end that decade NMR was routinely used as a central tool by synthetic organic chemists. Compared to other spectroscopies NMR spectra are embarrassingly easy to interpret and use as a tool for determining molecular structure. The frequency of each line tells you not only what type of atomic nuclei are present but can also distinguish among the same type of nuclei in different chemical bonding environments. Additionally, the intensity of each signal is quantitative. What could be simpler? With increasing magnetic field strengths, the separation between frequencies (in Hertz) increases, and thus, the ability to resolve overlapping peaks improves and larger molecules can be studied. Higher magnetic field strengths also offer significant improvements in sensitivity.

In the early years most NMR spectrometers were continuous-wave instruments. Today, practically all NMR experiments are performed as pulsed time domain Fourier transform experiments. We will examine the reasons for this situation later. It would be difficult and unnecessary to discuss all the NMR experiments (pulse sequences) that have been developed and applied over the years. The aim of

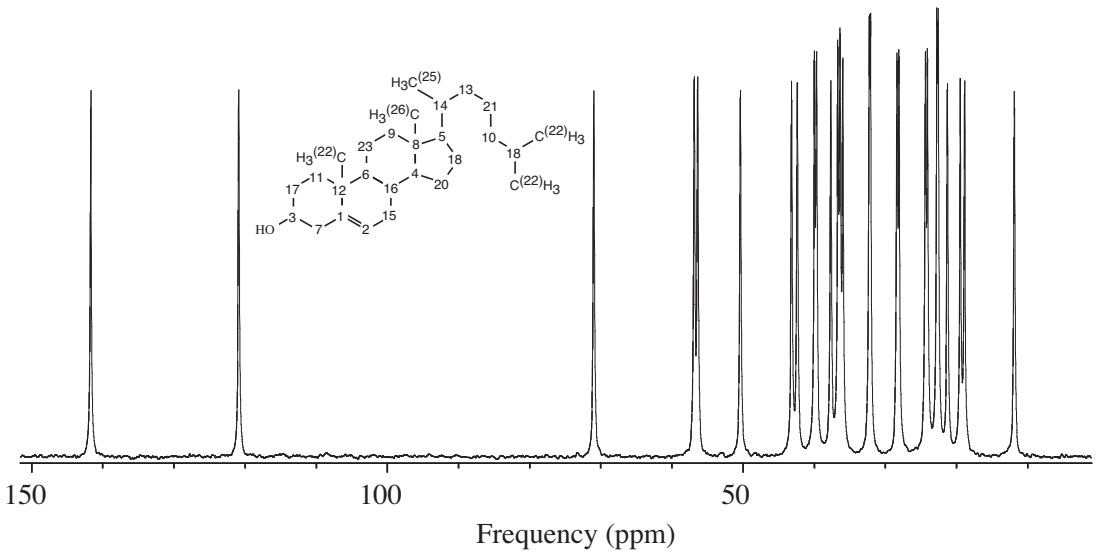

Figure 1.1: ^{1}H-*decoupled* ^{13}C *NMR spectrum of Cholesterol. There are 26 resonances in this spectrum, which when numbered from left to right, are assigned to the corresponding numbered carbon atom in Cholesterol based on its resonance frequency.*

P. J. Grandinetti, November 23, 2009

this text is to give you a basic understanding of the underlying theoretical and experimental aspects of the technique. With this understanding you should be able to follow many articles in the NMR literature and know how to implement most NMR experiments on a modern NMR spectrometer and analyze the data.

In this chapter, we will present a simple classical model for understanding the NMR experiment, intentionally avoiding the use of quantum mechanics so that a broader range of students can more quickly understand many key concepts behind the technique. In later chapters, we will review the necessary aspects of the quantum theory and connect them to the concepts described in this chapter.

1.2 Precessing Tops and the Faraday Detector

Let's start with the example of a macroscopic size spinning top in a gravitational field.

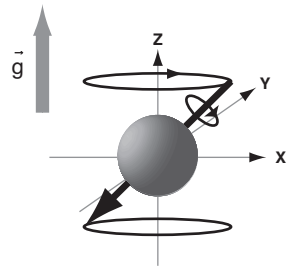

The top will precess about the direction of the gravitational field, with a characteristic frequency determined by parameters such as the mass, moments of inertia and the gravitational field strength, **g**. If we eliminate **g**, that is, place the top in a zero gravity environment, it will stop precessing. If we then insert a bar magnet inside our macroscopic top and placed it in a magnetic field, while still in a zero gravity environment,

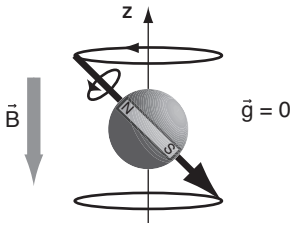

the "magnetic top" will precess about the direction of the magnetic field with a characteristic frequency ω_0 that is linearly proportional to the strength of the magnetic field B_0. In NMR, ω_0 is called the Larmor frequency, and the time of one precession is called the Larmor period.

How might one measure the precession frequency for a magnetic top? One way is to exploit Faraday's Law. Recall that a changing magnetic field will induce a current in a surrounding loop of wire. Thus, we place a coil of wire of radius r_{coil} around our spinning magnetic top.

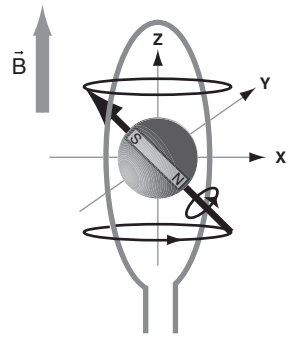

Faraday's Law tells us that the Electromotive Force (EMF, *i.e.*, voltage) induced in the coil will be related to the change in magnetic flux with time.

$$\mathcal{E} = -\frac{d\Phi}{dt} \tag{1.1}$$

Here $\mathcal{E}$ is the EMF and Φ is the magnetic flux. In our example, the magnetic dipole vector of the top will be changing with time according to

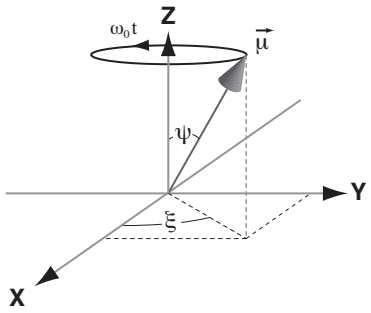

$$\boldsymbol{\mu}(t) = |\boldsymbol{\mu}| \left[\sin\psi\cos(\omega_0 t + \xi_0)\ \mathbf{e}_x + \sin\psi\sin(\omega_0 t + \xi_0)\ \mathbf{e}_y + \cos\psi\ \mathbf{e}_z\right], \tag{1.2}$$

where $|\boldsymbol{\mu}|$ is the length of the precessing vector, ψ is the angle between the precessing vector and the z-axis, ξ_0 is the initial phase of the precessing vector, and ω_0 is the precession frequency. With our precessing magnetic dipole at the origin the EMF induced in the coil will be

$$\mathcal{E}_x(t) = -\frac{d\Phi_x(t)}{dt} = \omega_0 \frac{\mu_0}{2r_{coil}} |\boldsymbol{\mu}| \sin\psi\sin(\omega_0 t + \xi_0). \tag{1.3}$$

From this signal we can measure the precession frequency. Let's consider the factors that influence the amplitude of this EMF signal. First, we see that the amplitude is directly proportional to the magnetic dipole moment strength, $|\boldsymbol{\mu}|$. Next there is a scaling by $\sin\psi$, implying that the closer the magnetic dipole precesses to the z-axis, the smaller the EMF signal. There is also a scaling by the inverse of the coil radius, so that the EMF signal amplitude decreases with increasing coil radius. And finally, we note that the EMF signal amplitude increases with increasing precession frequency. Thus, we see part of the sensitivity advantage to having the highest possible static fields where the precession frequency will be greatest.

1.2.1 The Zeeman Interaction

Now we make the connection to NMR. Every NMR active nucleus (*i.e.,* its spin angular momentum quantum number, I, is not zero) can be thought as a microscopic magnetic top. When you place an

NMR active nucleus in a magnetic field, the coupling between its magnetic dipole vector and the magnetic field will cause a precession about the magnetic field direction at a frequency, which to first order, is determined by its gyromagnetic ratio and the external magnetic induction field, *i.e.,*

$$\omega_0 = -\gamma B_0.$$

This coupling is called the Zeeman interaction, and γ is the nuclear gyromagnetic ratio. Typical values for γ for selected nuclei are given in Table 1.1.

Nucleus	Spin	Natural Abundance (Percent)	gyromagnetic ratio γ (10^7 rad/T-s)	Quadrupole Moment Q (barns)	Frequency at $B_0 = 2.35$ Tesla $\omega_0/2\pi$ (MHz)
^{1}H	1/2	99.985	26.7519	-	100
^{2}H	1	0.015	4.1066	2.8×10^{-3}	15.351
^{3}H	1/2	-	28.5349779	-	106.663974
^{3}He	1/2	0.000137	-20.3801587	-	76.179437
^{6}Li	1	7.59	3.9371709	-0.808	14.716086
^{7}Li	3/2	92.41	10.3977013	-40.1	38.863797
^{11}B	3/2	80.42	8.5843	4.1×10^{-2}	32.089
^{13}C	1/2	1.108	6.7283	-	25.145004
^{14}N	1	99.634	1.9337792	0.02044	7.226329
^{15}N	1/2	0.37	-2.712	-	10.136783
^{17}O	5/2	0.037	-3.6279	-2.6×10^{-2}	13.561
^{19}F	1/2	100	25.181	-	94.094003
^{23}Na	3/2	100	7.08013	0.10	26.466
^{25}Mg	5/2	10	-1.63887	0.1994	6.121642
^{27}Al	5/2	100	6.9762715	0.1403	26.056888
^{29}Si	1/2	4.70	-5.3188	-	19.867184
^{31}P	1/2	100	10.8394	-	40.480737
^{35}Cl	3/2	75.53	2.6240	-0.10	9.809
^{69}Ga	3/2	60.108	6.438855	0.171	24.001253
^{71}Ga	3/2	39.892	8.181171	0.107	30.496576
^{67}Zn	5/2	4.1	1.676688	0.150	6.256819
^{87}Rb	3/2	27.835	8.786400	0.132	27.835
^{107}Ag	1/2	51.839	-1.0889181	-	4.047878
^{109}Ag	1/2	48.161	-1.2518634	-	4.653601
^{235}U	7/2	0.7200	-0.52	4.936	1.841000

Table 1.1: NMR Properties for selected nuclei obtained from www.webelements.com. 1 barn = 10^{-24} cm^2.

1.3 The Chemical Shift Interaction

The slight variations in the resonance frequencies in Fig. 1.1 are caused by the **nuclear shielding** effect. To account for this we write the precession frequency as

$$\omega = -\gamma(1-\sigma)B_0, \tag{1.4}$$

where σ is called the isotropic nuclear shielding. This term arises from surrounding electrons that slightly shield the nucleus from the full strength of the external magnetic field. σ is a dimensionless quantity that is typically on the order of 10^{-6}. Nuclear shieldings depends on a number of factors, and often increases with increasing local electron density around a nucleus.

While an NMR spectrometer can measure the precession frequency with extremely high precision and accuracy, a direct measurement of σ using Eq. (1.4) is problematic since it requires equally precise and accurate measurements of B_0, which is complicated by the need to take into account the sample's bulk magnetic suseptibiliy and shape. For this reason, it is more convenient to use the **Chemical Shift**, which is defined in terms of the difference between NMR frequency of a given resonance and the NMR frequency of a resonance in a reference compound, that is,

$$\delta_{\text{sample}} = \frac{\omega_{\text{sample}} - \omega_{\text{reference}}}{\omega_{\text{reference}}} \tag{1.5}$$

which defined in terms of the nuclear shielding is

$$\delta_{\text{sample}} = \frac{\sigma_{\text{reference}} - \sigma_{\text{sample}}}{1 - \sigma_{\text{reference}}}. \tag{1.6}$$

Often chemical shifts are reported in units of parts per million, obtained by multiplying δ by 10^6. In solution state NMR, an internal reference, that is, a compound homogeneously mixed into the sample, is often used. This is preferred over external references, since it eliminates the need to correct for bulk magnetic suseptibilities differences.

1.4 Magnetic Resonance, Coherence, and Relaxation

One of the main objectives in the NMR experiment is to measure the precession frequency of every chemically distinct nucleus in the sample. To do this, we place a coil around a sample in a strong magnetic field and measure the oscillating voltage induced in the coil by all the nuclear spins precessing. There is just one complication with this approach. When you place a sample in a magnetic field, all its nuclear magnetic dipole vectors will precess about the magnetic field direction, but there will be a random distribution of angles from the z-axis, and angles in the x-y plane, in other words, a random distribution of ψ and ξ. Imagine approximately 10^{20} nuclear magnetic dipole vectors pointing in random directions in three dimensions and all of them precessing about the external magnetic field.

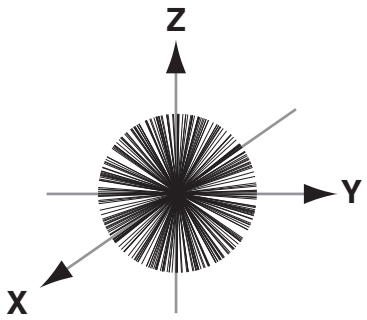

The vector sum of all the microscopic nuclear spin magnetic dipole vectors has a projection in the x-y plane of zero! Alas, there's no signal to detect with our Faraday detector. Fortunately, there is a solution. It turns out that after the sample comes to thermal equilibrium in the magnetic field, there are a few more nuclear magnetic dipole vectors on the $+z$ half of the sphere than the $-z$ half of the sphere, or if you change the sign of the gyromagnetic ratio, more vectors on the $-z$ half than the $+z$ half. Thus, there is a small non-zero vector sum pointing along the z-axis (*i.e.,* along the magnetic field direction). Here, we often say the spin system has Zeeman spin order. To a good approximation, the size of this vector from Zeeman spin order is related to the strength of the magnetic field according to

$$M_{eq} = \frac{1}{3}\frac{N\gamma^2\hbar^2 I(I+1)B_0}{k_B T},$$

where N is the total number of nuclei, I is the nuclear spin angular momentum, $\hbar$ is Planck's constant, k_B is Boltzmann's constant, and T is the temperature.

If the magnetization vector is along the z-axis it will give no signal. We need to find a way to move this net magnetization vector into the x-y plane[1]. One simple experimental solution is **Magnetic**

[1]In principle, one approach to do this would be to hop the magnetic field direction away from the magnetization suddenly. Then the net magnetization (still along the z-axis) would precess around the new magnetic field direction (now

Resonance, developed in the 1930's by I. I. Rabi, and for which he received the Nobel Prize in Physics in 1944. We start with the net magnetization vector lined up with the B_0 vector.

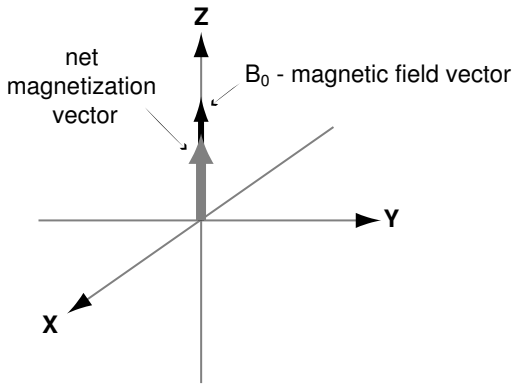

Then, we apply a second magnetic field, B_1, along the y-axis (which, in practice, is thousands of times smaller than B_0), so that the total external magnetic field vector now is ever so slightly tilted away from the z-axis.

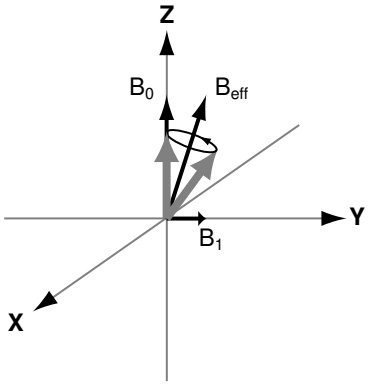

The net magnetization vector will begin precessing about this new effective magnetic field direction. After the magnetization has precessed 180° around the new effective magnetic field, we can switch the small B_1 to lie along the $-y$ axis.

perpendicular to the z-axis) and would then be detectable by a coil in the x-y plane. In practice, however, this is too difficult, since you would need to move the magnetic field direction much faster than one precession period, which in NMR would mean less than a nanosecond.

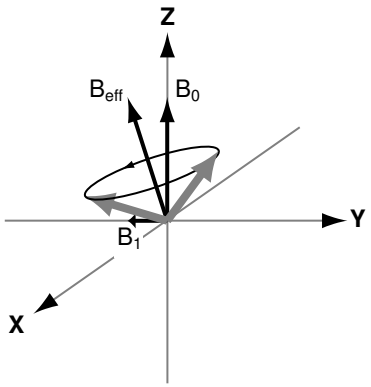

After switching the B_1 field direction, the magnetization vector will precess along a wider cone about the newer effective magnetic field direction. Once the net magnetization has processed 180° around this effective magnetic field direction, we switch the B_1 vector back along $+y$, and repeat the process. Eventually, we can take the net magnetization vector from along $+z$ and move it completely into the x-y plane. All we needed to accomplish this, was to apply a small alternating magnetic field along the y-axis that alternates with the same frequency that the net magnetization vector naturally precesses around the magnetic field direction. This process is called **magnetic resonance**. It allows us to take the net magnetization vector from along the z-axis and place it in the x-y plane[2].

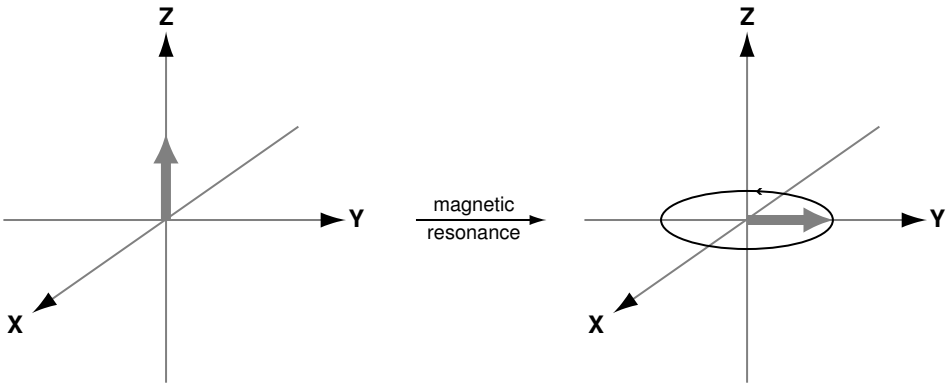

Once the magnetization vector is completely in x-y plane, we can turn off the alternating B_1 field and the magnetization will precess in the x-y plane and induce an EMF signal in a coil. We can even use

[2]Clearly to do a magnetic resonance experiment you need to know the precession frequency. You may be thinking that if you already knew the precession frequency why would you even bother doing the experiment? It turns out that you don't need to know the exact resonance frequency to do magnetic resonance. You can still move the magnetization vector away from the z-axis if you're slightly off resonance. Once there is a detectable magnetization component in the transverse plane, however, you will be able to measure the frequency very accurately with your detector coil.

the same coil that we use to receive the signal to generate the alternating B_1 magnetic field.

By taking the magnetization vector from the z axis to the x-y plane we have turned the Zeeman order of the spin system into a "coherence". The concept of coherence is central to understanding nearly all NMR experiments, so it is worthwhile to examine this concept more carefully. In NMR, coherence implies a correlated phase relationship among the orientations of many nuclear magnetic dipole vectors. Defined in this way, coherence has no meaning for a single nuclear spin[3] and is only a property of many nuclear spins in an ensemble. Consider an analogy to the "Mexican Wave"[4], a popular activity at football stadiums around the world. Let's say it takes one minute for the wave to travel around the stadium. One spectator alone standing up and then down once a minute will not create an observable wave. Likewise, all the spectators in the stadium standing up and down once a minute but each at random times will also not create an observable wave. It is only when there is a certain correlation between every spectator's standing cycle will there be an observable wave. The Mexican Wave requires "coherence" among many spectators to be observable.

In NMR there are relaxation processes that will destroy (randomize) the correlated phase relationship among the precessing nuclear magnetic dipole vectors in the sample, causing the spins to lose coherence. These relaxation processes, which randomize the phase relationships among the individual spin magnetic dipole vectors, eventually lead to the net magnetization being completely along the z-axis again. Two time constants often used to characterize these processes are:

T_2: **Spin-Spin (Transverse) Relaxation Time** - Time scale that coherence is lost in the x-y (transverse) plane.

T_1: **Spin-lattice (Longitudinal) Relaxation Time** - Time scale that the equilibrium net magnetization along the z (longitudinal) axis is restored.

So far, we've only considered the interaction of the nuclear magnetic dipole moment with the external magnetic fields, such as the static B_0, and the time dependent $B_1(t)$. Generally, a nucleus will experience a variety of interactions between all its electric and magnetic moments and its atomic and molecular surroundings (see section 1.8). NMR Relaxation arises from the time dependence of these interactions due to random molecular motion. For simplicity, we'll consider here just the interactions of an atom's nuclear magnetic dipole moment with the magnetic dipolar moments on neighboring atoms.

[3]Coherence can also defined as a correlated phase relationship for a single spin at different times. Do not confuse this usage with the one above, where there's a relationship among many spins at a given time.

[4]First became popular during the 1986 World Cup in Mexico. Spectators jump to their feet with arms outstretched - and sit down again as neighbors in the stand rise up.

Imagine a nuclear magnetic moment vector precessing about the external B_0 field on a cone of angle ψ. As neighboring molecules, containing their own nuclear magnetic moments, tumble and translate, they will generate a local oscillating magnetic field that can act on our nuclear magnetic moment vector and change not only the angle ψ about which it is precessing, but also advance or retard ξ, the phase of its precession. Although this process is happening to every nucleus in the sample, the phase and amplitude of the local field fluctuations experienced vary from nucleus to nucleus. This is the mechanism that destroys the phase coherence among the precessing nuclear spin magnetic moments and results in the T_2 decay of the transverse magnetization components, as well as the T_1 recovery of the equilibrium magnetization along the z axis. Note that T_1 relaxation is affected only by local fields that change the angle ψ, and not ξ, whereas T_2 relaxation is affected by local fields that change either ψ or ξ.

A nice feature of this simple picture for NMR relaxation is that it qualitatively explains the dependence of relaxation times on the time scale for molecular motion. When molecules are tumbling rapidly, such that the molecular correlation time τ is much shorter than the Larmor period, then the local field oscillation frequencies will be "off-resonant", and their ability to move a nuclear spin's magnetic moment vector away from the angle ψ will be diminished. Likewise, if the molecular correlation time τ is much longer than the Larmor period, the local field oscillations will again be "off-resonant" and less effective in reorienting the nuclear magnetic moment vector. It's only when the molecular correlation time is close to the Larmor period that we will find the most efficient relaxation, that is, the shortest T_1 value. Thus, we observe a minimum in the T_1 value as a function of molecular correlation time when $\omega_0\tau \approx 1$.

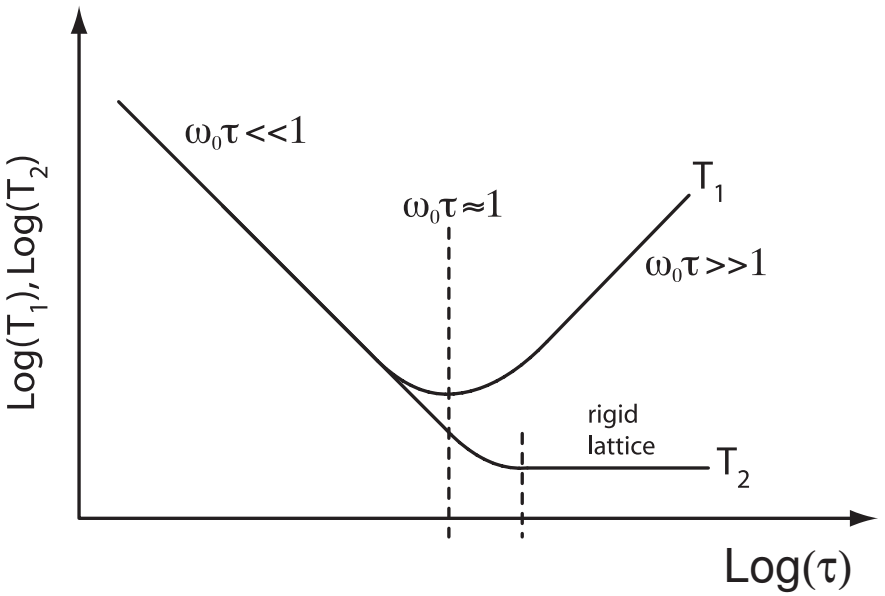

compound	nucleus	Temperature	Larmor Frequency	T_1 value or range
water	^{1}H	20° C	29 MHz	2.3 seconds
ethanol	^{1}H	20° C	29 MHz	2.2 seconds
glycerol	^{1}H	20° C	29 MHz	23 milliseconds
glycerol	^{2}D	20° C	9.2 MHz	2 seconds
chloroform-d	^{2}D	25° C	9.2 MHz	1.35 seconds
0.5 M sucrose in H_2O	^{13}C	27° C	15.08 MHz	1-2 seconds
methyl-cyclohexane	^{13}C	30° C	15.09 MHz	9-18 seconds

Table 1.2: Spin-lattice relaxation times, T_1, for selected substances.

Because T_2 relaxation is enhanced by any process that changes ξ, the phase of the spin precession it will also be affected by variations in static local fields, which can slow down or speed up the precession of the nuclear magnetic moment vectors. Such static local fields do not affect the precession angle ψ, only its phase, ξ. Thus, while T_1 relaxation is unaffected by static local fields, T_2 relaxation will not increase like T_1 in the long molecular correlation time limit. Eventually, the molecular correlation time becomes so slow that the sample becomes a rigid lattice, and then T_2 remains relatively constant. Note that T_1 will always be greater than or equal to T_2.

1.5 The Bloch Equations

We can calculate the magnetization vector in the NMR experiment with a vector sum of the individual nuclei's magnetic dipole moments according to

$$\mathbf{M}(t) = \sum_{j}^{N} \boldsymbol{\mu}_j(t). \tag{1.7}$$

In 1946 Felix Bloch proposed a phenomenological set of equations to describe the precession and relaxation of the net magnetization vector in the NMR experiment. Given a magnetization vector,

$$\mathbf{M}(t) = M_x(t)\mathbf{e}_x + M_y(t)\mathbf{e}_y + M_z(t)\mathbf{e}_z, \tag{1.8}$$

it will evolve according to

$$\frac{d\mathbf{M}(t)}{dt} = \boldsymbol{\omega}(t) \times \mathbf{M}(t) - [\mathbf{R}]\left[\mathbf{M}(t) - \mathbf{M}_{eq}\right], \tag{1.9}$$

where

$$\boldsymbol{\omega}(t) = -\gamma(1-\sigma)\mathbf{B}(t),$$

$$\mathbf{M}_{eq} = M_{eq}\,\mathbf{e}_z \quad \text{and} \quad [\mathbf{R}] = \begin{pmatrix} 1/T_2 & 0 & 0 \\ 0 & 1/T_2 & 0 \\ 0 & 0 & 1/T_1 \end{pmatrix}.$$

In the Bloch equations the $[\mathbf{R}]\left[\mathbf{M}(t) - \mathbf{M}_{eq}\right]$ term describes the relaxation decay of x-y "transverse" magnetization and the growth of z "longitudinal" magnetization (similar to first-order chemical kinetics). The $\boldsymbol{\omega}(t) \times \mathbf{M}(t)$ term describes the change in $\mathbf{M}(t)$ as it precesses about the $\mathbf{B}(t)$ direction. That is, the magnetization vector, $\mathbf{M}(t)$, precesses about the instantaneous direction of the vector $\boldsymbol{\omega}(t)$ with an instantaneous precession frequency specified by the length of the vector $\boldsymbol{\omega}(t)$.

The precession of the magnetization vector has so far been described with respect to a stationary reference frame associated with the lab. What if we stood on a turntable at the origin of our magnetization vector, and the turntable was spinning at the same angular velocity as the magnetization vector?

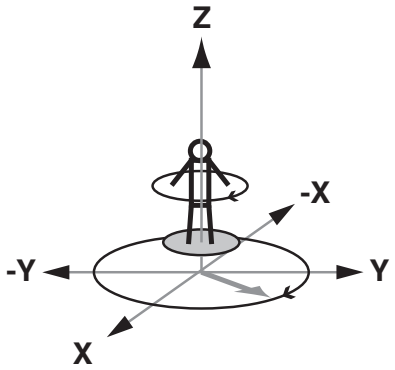

Then the lab frame would appear (to us) to be rotating in the opposite direction, and the magnetization would appear stationary in this "rotating frame". You can then imagine that the fast precessing and relaxing magnetization vector in the lab frame would not be precessing at all if your rotating frame exactly matched the precession frequency. That is, in the rotating frame the magnetization vector sum would just move from y^* to z^*, or if $T_1 \gg T_2$ the vector would shrink to zero along y^* and then grow to M_{eq} along z^*.

Transforming the Bloch Equations into this frame we obtain

$$\frac{d^*\mathbf{M}(t)}{dt} = \boldsymbol{\omega}_{eff}(t) \times \mathbf{M}(t) - [\mathbf{R}]\{\mathbf{M}(t) - \mathbf{M}_{eq}\}, \tag{1.10}$$

where the magnetization vector, $\mathbf{M}(t)$, precesses in the rotating frame about a direction with a lower precession frequency given by

$$\boldsymbol{\omega}_{eff}(t) = \boldsymbol{\omega}(t) - \boldsymbol{\omega}_{rot}. \tag{1.11}$$

Here $\boldsymbol{\omega}_{rot}$ arises from going into the "rotating frame". With Eq. (1.10), we can write the rate of change for the magnetization vector components in the rotating frame. Let's first start with the static magnetic field applied alone, and then consider the static field and an oscillating magnetic resonance field.

1.5.1 Free Precession

In the presence of a static magnetic field alone the rotating frame precession frequency will be

$$\Omega = \omega_0(1 - \sigma) - \omega_{rot}, \tag{1.12}$$

and the general solution for the magnetization in the rotating frame will be

$$\begin{pmatrix} M_x^*(t) \\ M_y^*(t) \\ M_z^*(t) \end{pmatrix} = \begin{pmatrix} \left[M_x^*(0)\cos\Omega t - M_y^*(0)\sin\Omega t\right] e^{-t/T_2} \\ \left[M_y^*(0)\cos\Omega t + M_x^*(0)\sin\Omega t\right] e^{-t/T_2} \\ M_z^*(0)e^{-t/T_1} + M_{eq}(1 - e^{-t/T_1}) \end{pmatrix}, \tag{1.13}$$

where M_x^*, M_y^*, and M_z^* are the magnetization vector components in the rotating frame.

When describing free precession it is often convenient to define the magnetization vector in NMR in terms of spherical basis vectors, that is,

$$\mathbf{M}(t) = M_{+1}^*(t)\mathbf{e}^{+1} + M_0^*(t)\mathbf{e}^0 + M_{-1}^*(t)\mathbf{e}^{-1},$$

where $\mathbf{e}^q$ are defined by

$$\mathbf{e}^{\pm 1} = \mp\frac{1}{\sqrt{2}}(\mathbf{e}_x \mp i\mathbf{e}_y), \quad \mathbf{e}^0 = \mathbf{e}_z, \tag{1.14}$$

and the components M_q are given by

$$M_{\pm 1} = \mp\frac{1}{\sqrt{2}}(M_x \pm iM_y), \quad M^0 = M_z. \tag{1.15}$$

Note the sign difference in the definition of $\mathbf{e}^{\pm 1}$ and $M_{\pm 1}$. With this definition the general solution for free precession of the transverse components becomes

$$M_{\pm 1}^*(t) = M_{\pm 1}^*(0)e^{\pm i\Omega t}e^{-t/T_2}.$$

Using spherical basis vectors gives us a more compact means for describing the length, orientation in the x-y plane, and sense of rotation about the z-axis of the transverse components of the magnetization vector. Most importantly, note that other than being multiplied by a phase factor $e^{\pm i\Omega t}$, *the* $M_{\pm 1}^*$ *components are unaffected by rotation about the* z*-axis.*

The signal detected in the NMR experiment, written in terms of the magnetization components in the rotating frame, is given by

$$S(t) = kM_{+1}^*(t)e^{i\phi_{ref}}, \tag{1.16}$$

where ϕ_{ref} is the receiver reference phase and k is a constant that depends on the receiver coil geometry and the receiver frequency.

1.5.2 An RF Pulse

Now we consider the more difficult case of the static field and a magnetic field oscillating at a frequency $|\omega_{rf}|$, which is always defined as positive. In the lab frame, we have

$$\mathbf{B}(t) = 2B_1\cos(|\omega_{rf}|t + \psi_{rf})\mathbf{e}_x + B_0\mathbf{e}_z. \tag{1.17}$$

Taken into the rotating frame we obtain[5] an time independent expression for $\boldsymbol{\omega}_{eff}$,

$$\boldsymbol{\omega}_{eff} = \omega_1[\cos\phi\,\mathbf{e}_x^* + \sin\phi\,\mathbf{e}_y^*].$$

[5]Here, we have defined the nutation or Rabi frequency as $\omega_1 = |\gamma B_1|$, and have redefined the phase of radio frequency (rf) as $\phi = -(\text{sign }\gamma)\,\psi_{rf}$ to yield an expression for $\boldsymbol{\omega}_{eff}$ that is independent of the sign of γ.

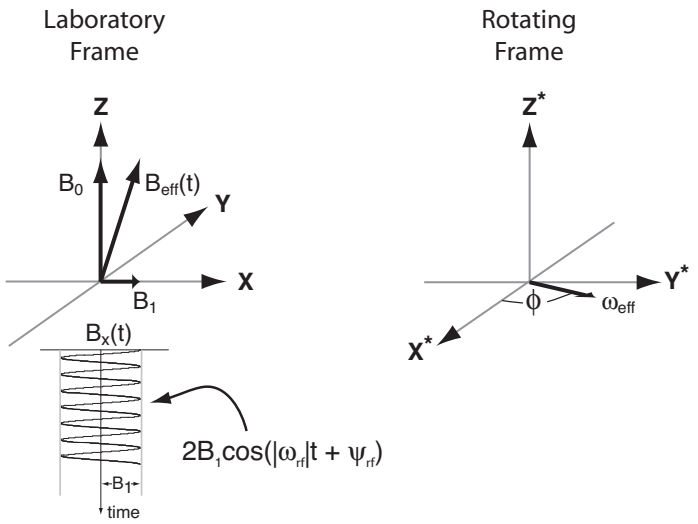

If the rf phase is set to $\phi = 0$, then we get a solution for the transformation of $\mathbf{M}(0)$ into $\mathbf{M}(t)$

$$\boxed{\begin{pmatrix} M_x^* \\ M_y^* \\ M_z^* \end{pmatrix} \xrightarrow{\mathbf{R}_{x(\omega_1 t)}} \begin{pmatrix} M_x^* \\ M_y^* \cos\omega_1 t - M_z^* \sin\omega_1 t \\ M_z^* \cos\omega_1 t + M_y^* \sin\omega_1 t \end{pmatrix} \begin{matrix} \text{rf pulse} \\ \text{along } x^*\text{-axis} \\ (\phi = 0), \end{matrix}} \tag{1.18}$$

Thus, the magnetic resonance approach to moving the magnetization from along z^* to the x^*-y^* plane is seen as a simple rotation about a single axis in the rotating frame. A magnetization vector initially along the $+z^*$ axis will be rotated counterclockwise to the $-y^*$ axis after a time $\omega_1 t = \pi/2$.

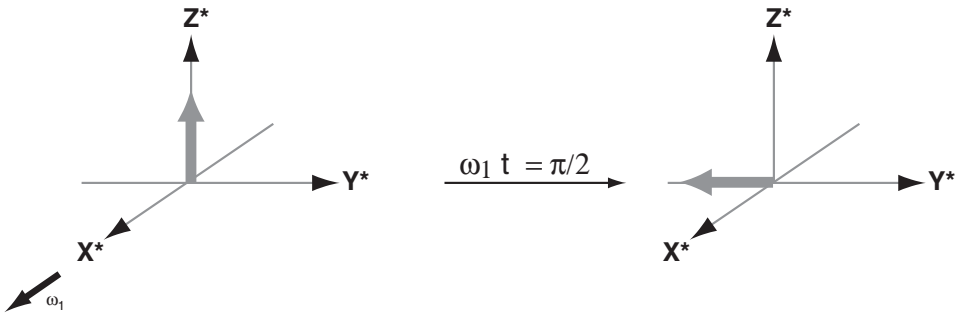

The time is called a 90° (or $\pi/2$) pulse length in NMR. The maximum signal will be detected in the receiver coil after a 90° pulse.

If you turned the *rf* pulse on long enough so that $\omega_1 t = \pi$, then you could also rotate the magnetization from $+z^*$ to $-z^*$.

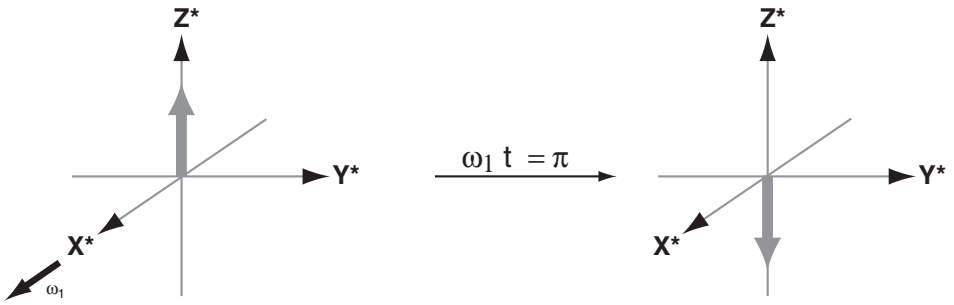

This is called a π-pulse (180°-pulse). In the specific case when magnetization is taken from $+z^*$ to $-z^*$, it is called an **inversion pulse**. After an inversion pulse, there will be no detectable signal in the receiver coil. In practice, the strength of the ω_1 is determined experimentally by systematically increasing the pulse length until a full oscillation in signal strength is observed.

Similarly, if we set $\phi = \pi/2$, then we would have a transformation of $\mathbf{M}(0)$ into $\mathbf{M}(t)$ according to

$$\boxed{\begin{pmatrix} M_x^* \\ M_y^* \\ M_z^* \end{pmatrix} \xrightarrow{\mathbf{R}_{y(\omega_1 t)}} \begin{pmatrix} M_x^* \cos\omega_1 t + M_z^* \sin\omega_1 t \\ M_y^* \\ M_z^* \cos\omega_1 t - M_x^* \sin\omega_1 t \end{pmatrix} \begin{array}{c} \text{rf pulse} \\ \text{along } y^*\text{-axis} \\ (\phi = \pi/2). \end{array}} \tag{1.19}$$

Setting $\omega_1 t = \pi/2$ with $\phi = \pi/2$ gives a counterclockwise rotation about the y^*-axis which will rotate a magnetization vector along $+z^*$ to the $+x^*$ axis.

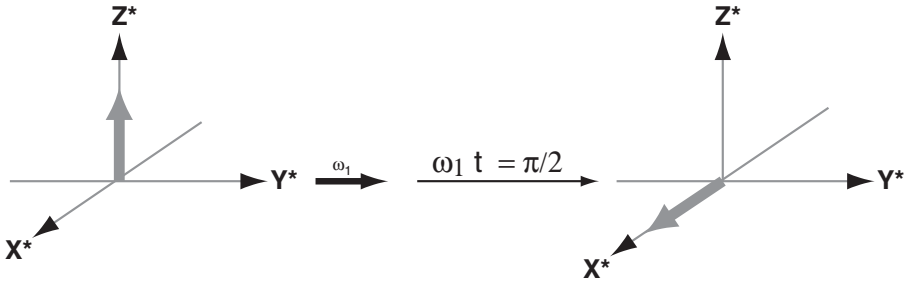

Finally, let's consider the effect of an rf pulse of arbitrary phase on the magnetization vector expressed in terms of the spherical basis vector components. We find the effect of a $\pi/2$ pulse of arbitrary phase to be

$$\begin{pmatrix} M_{+1}^* \\ M_0^* \\ M_{-1}^* \end{pmatrix} \xrightarrow{\mathbf{R}_{\phi(\pi/2)}} \begin{pmatrix} \frac{1}{2}M_{-1}^* e^{i2\phi} & -\frac{i}{\sqrt{2}}M_0^* e^{i\phi} & +\frac{1}{2}M_{+1}^* \\ \frac{i}{\sqrt{2}}M_{-1}^* e^{i\phi} & & -\frac{i}{\sqrt{2}}M_{+1}^* e^{-i\phi} \\ \frac{1}{2}M_{-1}^* & +\frac{i}{\sqrt{2}}M_0^* e^{-i\phi} & +\frac{1}{2}M_{+1}^* e^{-i2\phi} \end{pmatrix} \tag{1.20}$$

and the effect of a π pulse of arbitrary phase to be

$$\begin{pmatrix} M_{+1}^* \\ M_0^* \\ M_{-1}^* \end{pmatrix} \xrightarrow{\mathbf{R}_{\phi}(\pi)} \begin{pmatrix} M_{-1}^* e^{i2\phi} \\ -M_0^* \\ M_{+1}^* e^{-i2\phi} \end{pmatrix}. \tag{1.21}$$

Notice that the transverse components of the magnetization vector in the spherical unit vector bases, that is, M_{+1}^* and M_{-1}^*, are swapped by a π pulse,

In the literature, one often sees the following notations in NMR:

- $(\pi/2)_y$ which means a $\omega_1 t = \pi/2$ pulse of B_1 along the y-axis of the rotating frame
- $(\pi/2)_x$ which means a $\omega_1 t = \pi/2$ pulse along x-axis of rotating frame
- $(\pi/2)_{\overline{y}}$ or $(\pi/2)_{-y}$ which means a $\omega_1 t = \pi/2$ pulse along $-y$ axis of rotating frame
- $(\pi)_x$ which means a $\omega_1 t = \pi$ pulse along the x-axis of the rotating frame

Generally, one writes $(\beta)_\phi$ where $\beta = \omega_1 t$ and ϕ is the rf pulse phase, that is,

$$\begin{aligned} \phi = &\quad 0^\circ &\rightarrow &\quad x \\ \phi = &\quad 90^\circ &\rightarrow &\quad y \\ \phi = &\quad 180^\circ &\rightarrow &\quad -x \\ \phi = &\quad 270^\circ &\rightarrow &\quad -y \end{aligned}$$

1.5.3 The Bloch Decay

Now let's consider the trajectory of the magnetization vector in the simplest NMR experiment: A single $(\pi/2)_x$ pulse followed by acquisition of the NMR signal. Since we will ultimately be detecting the complex magnetization component $M_{+1}(t)$ in the rotating frame with our receiver coil it is more convenient to follow the trajectory of the magnetization vector expanded in terms of the spherical basis vectors. The

evolution of the magnetization during this experiment will go as follows:

$$\mathbf{M} = \underbrace{M_{eq}}_{M_0}\,\mathbf{e}_0.$$

$$\Big\downarrow (\pi/2)_x$$

$$\mathbf{M}^\dagger = \underbrace{-M_{eq}}_{M_y^{*\dagger}}\mathbf{e}_y = \underbrace{\frac{i}{\sqrt{2}}M_{eq}}_{M_{-1}^{*\dagger}}\,\mathbf{e}^{-1} + \underbrace{\frac{i}{\sqrt{2}}M_{eq}}_{M_{+1}^{*\dagger}}\,\mathbf{e}^{+1}$$

$$\Big\downarrow \text{free evolution}$$

$$\mathbf{M}(t) = \underbrace{\frac{i}{\sqrt{2}}M_{eq}e^{-i\Omega t}e^{-t/T_2}}_{M_{-1}^*(t)}\,\mathbf{e}^{-1} + \underbrace{M_{eq}(1-e^{-t/T_1})}_{M_0^*(t)}\,\mathbf{e}^{0} + \underbrace{\frac{i}{\sqrt{2}}M_{eq}e^{i\Omega t}e^{-t/T_2}}_{M_{+1}^*(t)}\,\mathbf{e}^{+1}.$$

We obtain the signal detected in this experiment by plugging the $M_{+1}^*(t)$ component into Eq (1.16). Setting the receiver phase, ϕ_{ref}, to zero, we obtain

$$S(t) = -\frac{i}{\sqrt{2}}kM_{eq}e^{i\Omega t}e^{-t/T_2} = S(0)e^{i\Omega t}e^{-t/T_2}. \tag{1.22}$$

The time dependent signal after a single $\pi/2$ pulse is called a Bloch Decay, or more commonly known as the Free Induction Decay (FID).

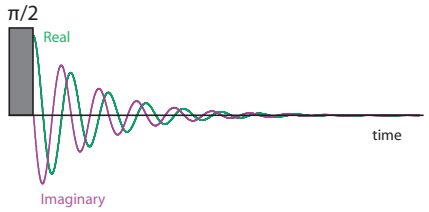

1.6 The Fourier Transform

The time domain free induction decay and the NMR spectrum are related by the Fourier transform. Most everyone is familiar with the idea behind this transform. For example, in music a sound is represented as a note on a staff representing frequencies. When you hear a note your ear is sensing oscillations in air density, and your brain recognizes what frequency it is.

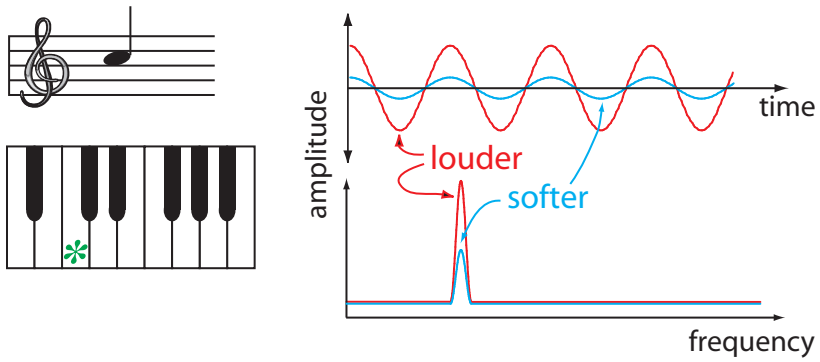

The louder the note, the bigger the amplitude of the sound wave you hear. Also the higher the note, the higher the frequency of sound oscillations you hear.

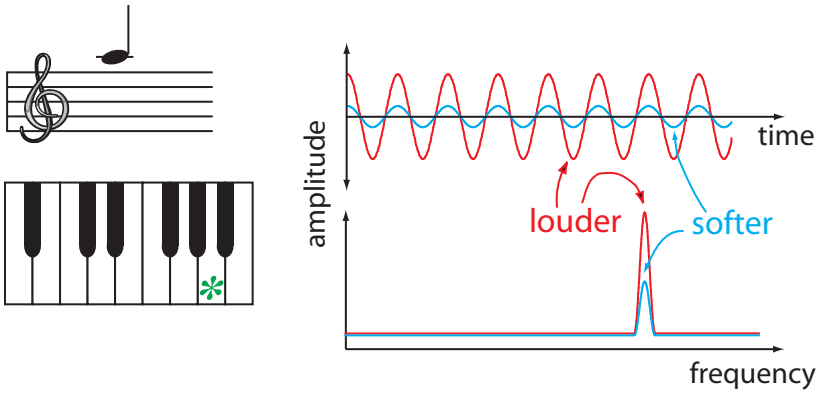

So we can view a musical note as either a time domain signal or frequency domain signal. Now, if you have a good musical ear, you might be able to listen to more than one note simultaneously and be able to distinguish more than one frequency.

P. J. Grandinetti, November 23, 2009

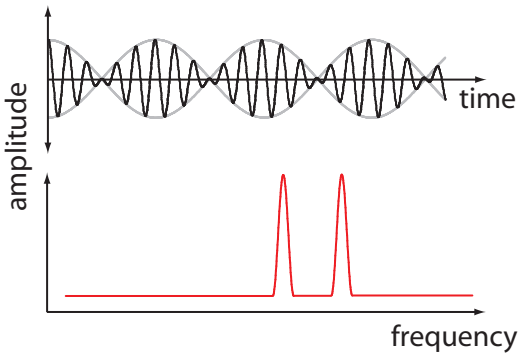

What Fourier realized was how to mathematically relate some oscillating signal (like sound) and transform it into a plot of amplitude versus frequency, that is

$$S(\omega) = \int_{-\infty}^{\infty} S(t) e^{-i\omega t} dt. \tag{1.23}$$

We integrate $S(t)$ over all time for each ω to get $S(\omega)$. $S(t)$ and $S(\omega)$ are called the time and frequency domain signals, respectively. The **inverse Fourier transform**

$$S(t) = \frac{1}{2\pi} \int_{-\infty}^{\infty} S(\omega) e^{i\omega t} d\omega \tag{1.24}$$

takes you from the frequency domain signal to the time domain signal. $S(\omega)$ and $S(t)$ form a Fourier transform pair. Let's take the signal

$$S(t) = \cos \Omega t = \frac{1}{2}[e^{i\Omega t} + e^{-i\Omega t}] \tag{1.25}$$

as an example.

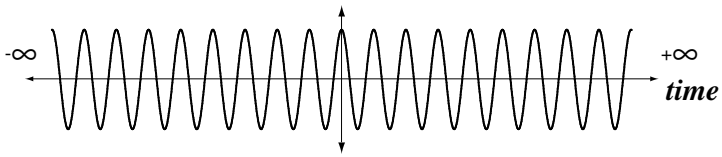

The Fourier transform of this signal is calculated according to

$$S(\omega) = \int_{-\infty}^{\infty} S(t)\, e^{-i\omega t} dt = \frac{1}{2} \int_{-\infty}^{\infty} e^{i\Omega t} e^{-i\omega t} dt + \frac{1}{2} \int_{-\infty}^{\infty} e^{-i\Omega t} e^{-i\omega t} dt,$$

and becomes

$$S(\omega) = \frac{1}{2}\delta(\Omega - \omega) + \frac{1}{2}\delta(-\Omega - \omega),$$

where

$$\delta(x) = \begin{cases} \infty & \text{if} \quad x = 0 \\ 0 & \text{if} \quad x \neq 0 \end{cases}$$

So the Fourier transform of $S(t) = \cos \Omega t$ looks like

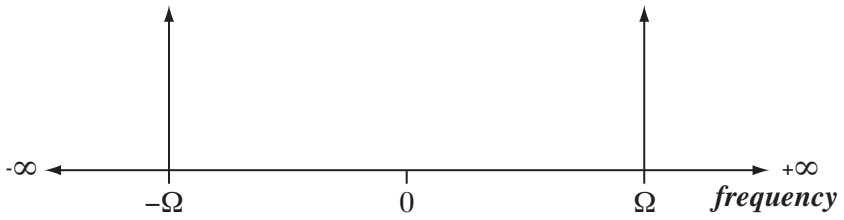

i.e., a spike at Ω and $-\Omega$ and zero everywhere else.

In this context a negative frequency has little meaning. However, in the context of the rotating frame, we can connect this with the sense of circular motion of magnetization vectors. Here's an example of counter clockwise motion in the complex plane.

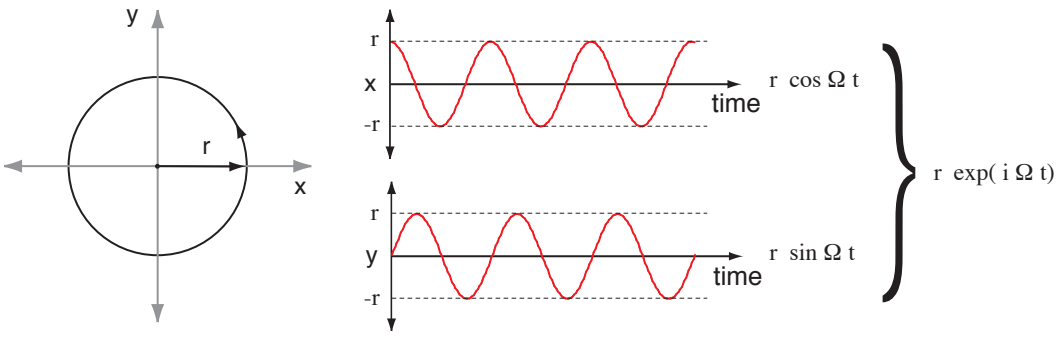

A point in the complex plane is defined $z = x + iy$ or in polar coordinates $z = re^{-i\theta}$. The Fourier transform of this complex signal is

$$re^{i\Omega t} \overset{FT}{\rightarrow} r\delta(\Omega - \omega)$$

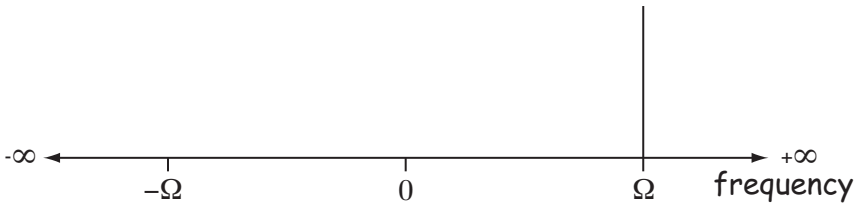

Likewise clockwise motion in the complex plane is described by

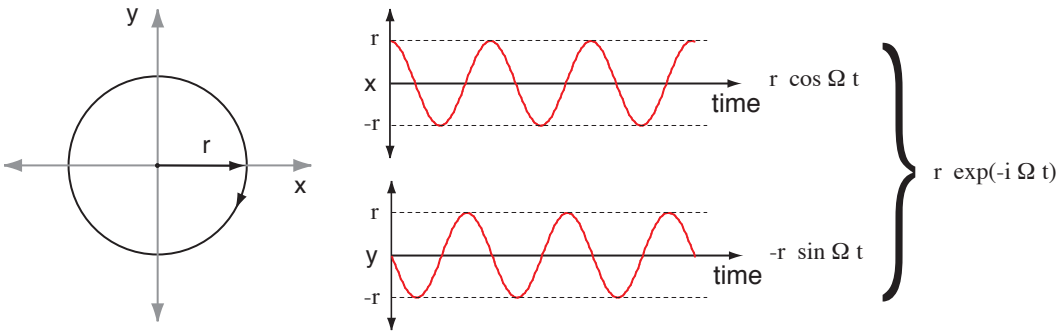

and the Fourier transform of this complex signal is

$$re^{i\Omega t} \stackrel{FT}{\rightarrow} r\delta(-\Omega - \omega).$$

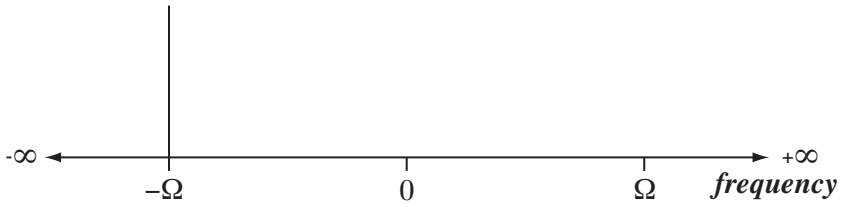

In a rotating frame those magnetization vectors precessing slower than the rotating frame will appear to rotate in the opposite direction of those precessing faster than the rotating frame.

Now let's look at something more realistic - more like NMR, *i.e.,* a signal that starts at time $t = 0$ and decays exponentially with time.

$$S(t) = e^{i\Omega t}e^{-t/T_2}$$

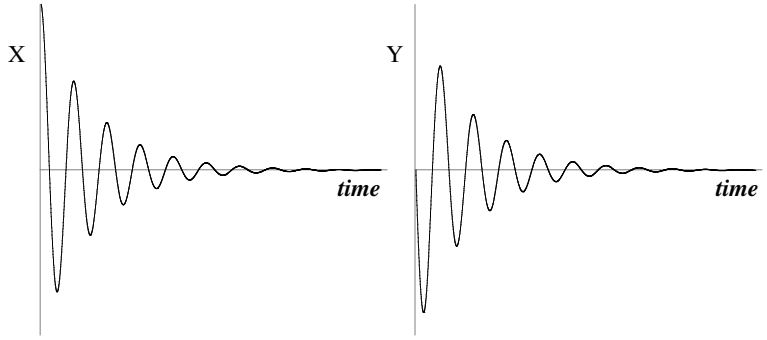

In this case the limits of our integral go from zero to $+\infty$, not $-\infty$ to $+\infty$.

$$\begin{aligned} S(\omega) &= \int_0^\infty e^{i\Omega t}e^{-t/T_2}e^{-i\omega t}dt \\ &= \frac{1/T_2}{(1/T_2)^2 + (\Omega - \omega)^2} + i\,\frac{(\Omega - \omega)}{(1/T_2)^2 + (\Omega - \omega)^2} \end{aligned}$$

Our spectrum has a real and an imaginary part. The real part is called the Absorption mode spectrum and the imaginary part is called the Dispersion mode spectrum.

$$\begin{aligned} A(\omega) &= \frac{\lambda}{\lambda^2+\omega^2}; \qquad \text{Absorption Mode Lineshape} \\ D(\omega) &= \frac{\omega}{\lambda^2+\omega^2}; \qquad \text{Dispersion Mode Lineshape} \end{aligned} \tag{1.26}$$

Here $\lambda = 1/T_2$.

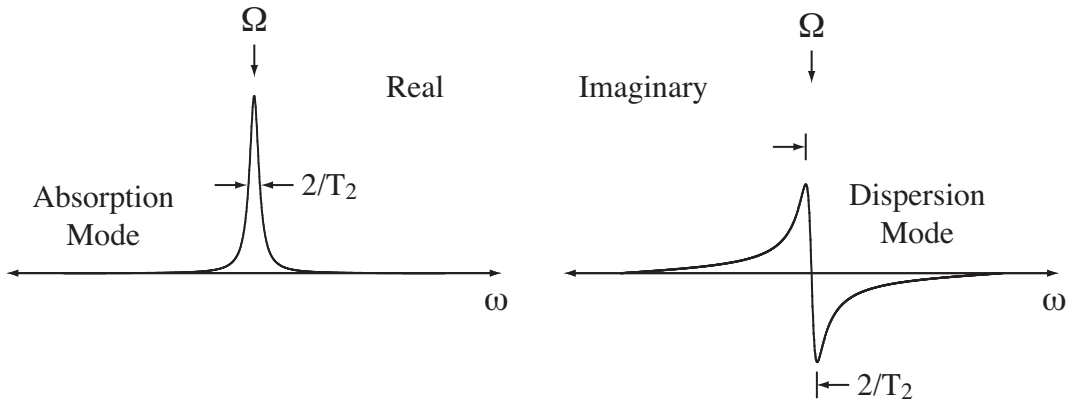

As you can see from these equations, while the lineshapes associated with the real and imaginary parts of the NMR spectrum are different, they contain the same information. They are related by the Kramers-Kronig relation

$$A(\omega) = \frac{1}{\pi}\int_{-\infty}^{\infty}\frac{D(\omega')}{\omega-\omega'}d\omega' \qquad \text{and} \qquad D(\omega) = -\frac{1}{\pi}\int_{-\infty}^{\infty}\frac{A(\omega')}{\omega-\omega'}d\omega'. \tag{1.27}$$

The tails of the dispersion lineshape extend further out than the absorption lineshape. These lineshapes are characteristic of any damped oscillator problem. The names absorption and dispersion come from optical spectroscopies. Generally, the specific form of the absorption- and dispersion-mode lineshape functions in an NMR spectrum can vary depending on the system under study. Our particular example has an exponentially decaying signal, whose well-known Fourier transform results in a **Lorentzian lineshape** in the Absorption mode. For a Lorentzian lineshape the **full width at half height**, Γ, is equal to $2/T_2$. Another common Fourier transform "pair" is the Gaussian decaying signal, whose Fourier transform is a Gaussian lineshape in the Absorption mode. Gaussian lineshapes tend to arise when there is a distribution in resonance frequencies. That is, when the signal arises from many transitions, each having ever so slightly different transition frequencies, then the overall lineshape becomes Gaussian.

This is often explained in terms of the Central Limit Theorem[6]. Lorentzian lineshapes are observed in liquid state NMR spectra, whereas Gaussian lineshapes are more common in solid-state NMR spectra.

1.6.1 Phase Corrections

Whenever you have complex signals you always have the issue of the phase relationship between the real and imaginary parts. Recall the relationships

$$z = x + iy = re^{i\phi}, \tag{1.28}$$

where

$$\phi = \tan^{-1}\frac{y}{x} \quad \text{and} \quad r = \sqrt{x^2 + y^2}. \tag{1.29}$$

In our context of circular motion in the complex plane we have a vector rotating where r is the length of the vector and ϕ is the angle from the x axis.

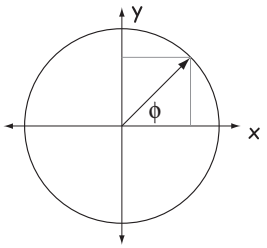

Let's look at how this picture is used in NMR, and how it relates to phase corrections of NMR spectra. Immediately after applying a $\pi/2$ pulse along the y axis the magnetization previously along z will now be along the x axis, and begins precessing in the x-y plane of the rotating frame. If we plotted the tip of the net magnetization vector in the x-y plane as it evolved we would see

[6]This theorem says that when you have many different contributions to the lineshape, each with their own characteristic lineshape, then in the limit that you have a infinite number of contributions the final lineshape will be Gaussian, even if none of the individual lineshapes are Gaussian. An important condition is that the component have the same order of magnitude and that no single source dominates all the others.

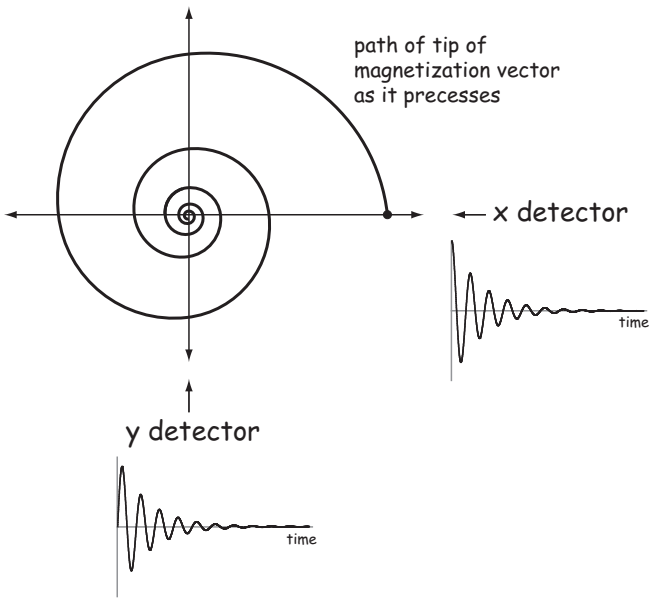

1.6.1.1 Zeroth Order Phase Correction

What happens if the magnetization doesn't start out exactly lined up with the x-axis at $t = 0$, but rather is offset from the x-axis by an angle ϕ?

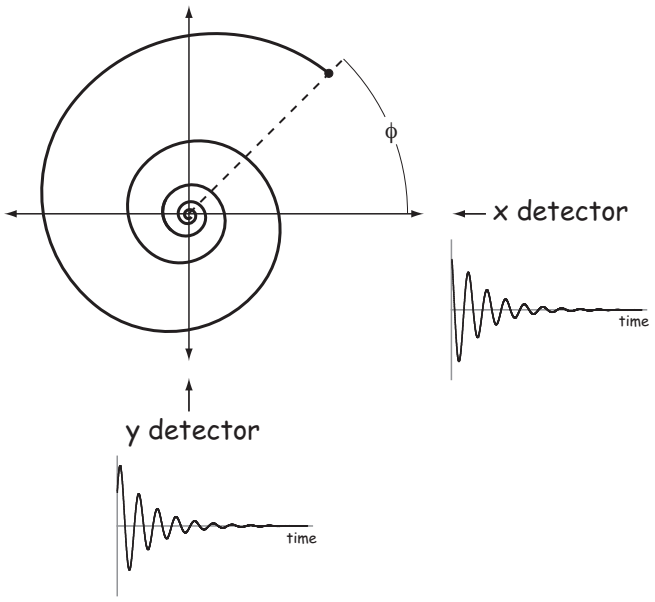

The complex Fourier transform of this signal may look like

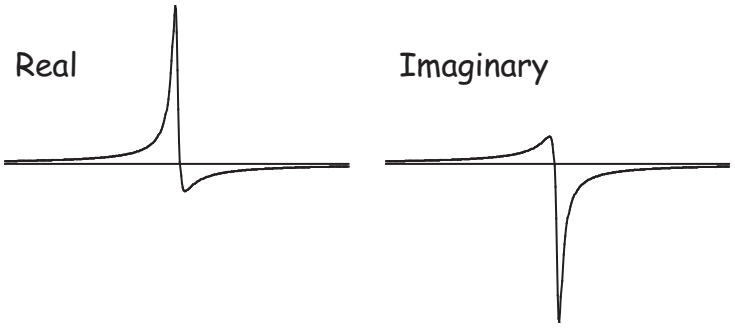

and neither of these look like absorption or dispersion mode signals. In this case we can calculate what is in the real and imaginary parts. It is given by

$$S(\omega) = [A(\omega - \Omega) + iD(\omega - \Omega)]e^{i\phi} \tag{1.30}$$

which can be expanded out to

$$S(\omega) = \underbrace{[A(\omega - \Omega)\cos\phi - D(\omega - \Omega)\sin\phi]}_{\text{real part}} + \underbrace{i[A(\omega - \Omega)\sin\phi + D(\omega - \Omega)\cos\phi]}_{\text{imaginary part}}. \tag{1.31}$$

One can show that when $\phi = \pi/2$ (*i.e.,* magnetization starts precessing from along the y axis), then the Fourier transform of the resulting signal will be

$$S(\omega) = -D(\omega - \Omega) + iA(\omega - \Omega). \tag{1.32}$$

Since the conventional in NMR is to report only the absorption mode spectrum it is standard procedure to apply a phase correction to the spectrum (or fid) so that the real part of the spectrum contain only the absorption mode spectrum. The spectrum is corrected by the simple application of a zeroth order phase correction,

$$S'(\omega) = S(\omega)e^{-i\phi_0}, \tag{1.33}$$

where ϕ_0 is adjusted until $\phi_0 = -\phi$ and the spectrum contains pure absorption mode lineshapes in the real part.

1.6.1.2 First Order Phase Correction

Now let's consider when we have two or more resonances present in the spectrum. In a given time the magnetization for site 2 will have rotated further around than the magnetization for site 1. For example, think of two athletes running around a track. At the starting line they are in-phase with each other. After they start running, the faster runner will be further along the track than the slower runner so

there will be a phase difference. In principle, this is no problem since they both start out at the same point and the Fourier transform gives pure absorption mode spectra for both sites in the real part and pure dispersion mode spectra for both sites in the imaginary part.

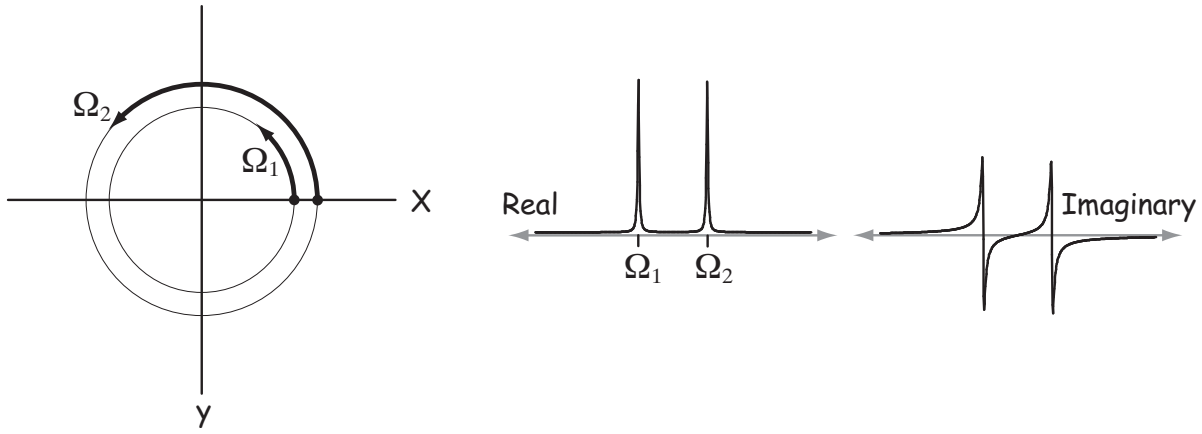

Even if our detector is 45° away from the starting point then we phase correct the spectrum to get the pure absorption mode in real and pure dispersion mode in the imaginary part. The problem comes in if you're late and miss the starting point. That is, you turn your detector on at the some time t_0 after the starting point. Then what you may see is ...

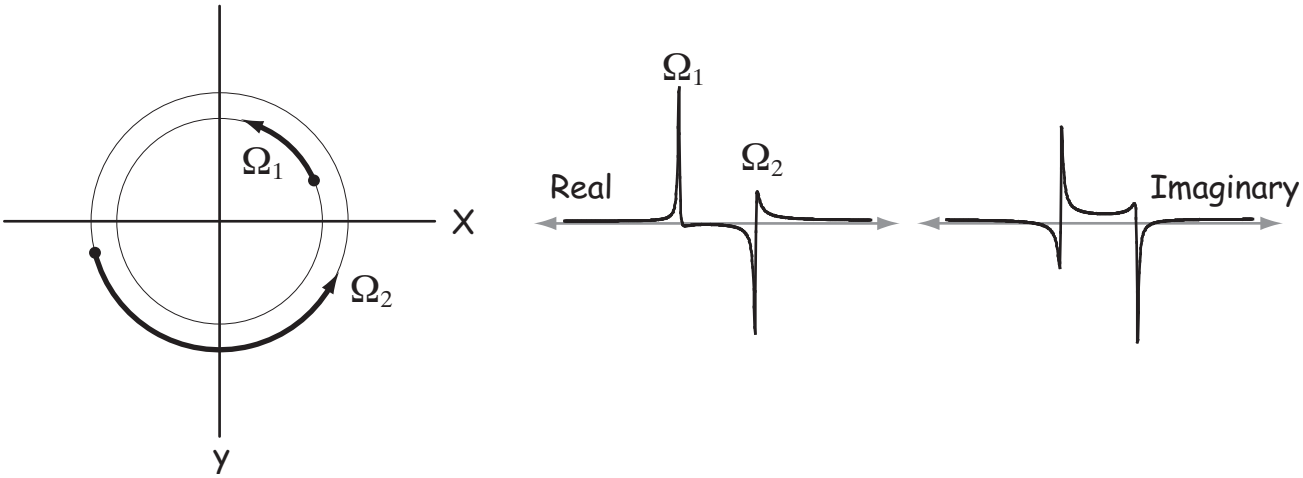

Site 2 had precessed significantly ahead of site 1 before the receiver was turned on. Now the phase we need to make site 1 have a pure absorption mode spectrum in the real part is not the same as the phase needed for site 2. The phase correction we need can be calculated from the frequency of each site. Thus,

we define our phase correction as linearly dependent on ω,

$$\underbrace{\phi(\omega)}_{\text{total phase}} = \underbrace{\phi_0}_{\text{0th order}} + \underbrace{\omega t_0}_{\text{1st order}} \tag{1.34}$$

where t_0 is the time we were late in starting the detector. Each frequency in the spectrum gets a different phase correction. Thus, we apply

$$S'(\omega) = S(\omega)e^{i\phi_0}e^{i\omega t_0}, \tag{1.35}$$

to obtain a spectrum with both sites in pure absorption mode in the real part of the spectrum. Applied to our example, we obtain

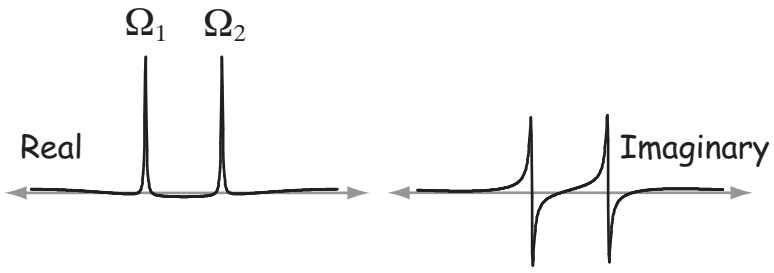

Actually, you get pure absorption mode lineshape in the real part plus a sinc-type function distortion in the baseline. Remember that the time shift theorem says that a time shift can be effected by a phase shift in the frequency domain.

$$S(t - t_0) \overset{F.T.}{\leftrightarrow} S(\omega)e^{i\omega t_0} \tag{1.36}$$

So, in effect, by applying the phase shift to get pure absorption mode spectrum you are shifting the time domain signal so that the time origin is where it should have been, which we can see from the convolution theorem is like multiplying a "correctly" acquired (*i.e.,* acquisition started at $t = 0$) signal by a step function.

P. J. Grandinetti, November 23, 2009

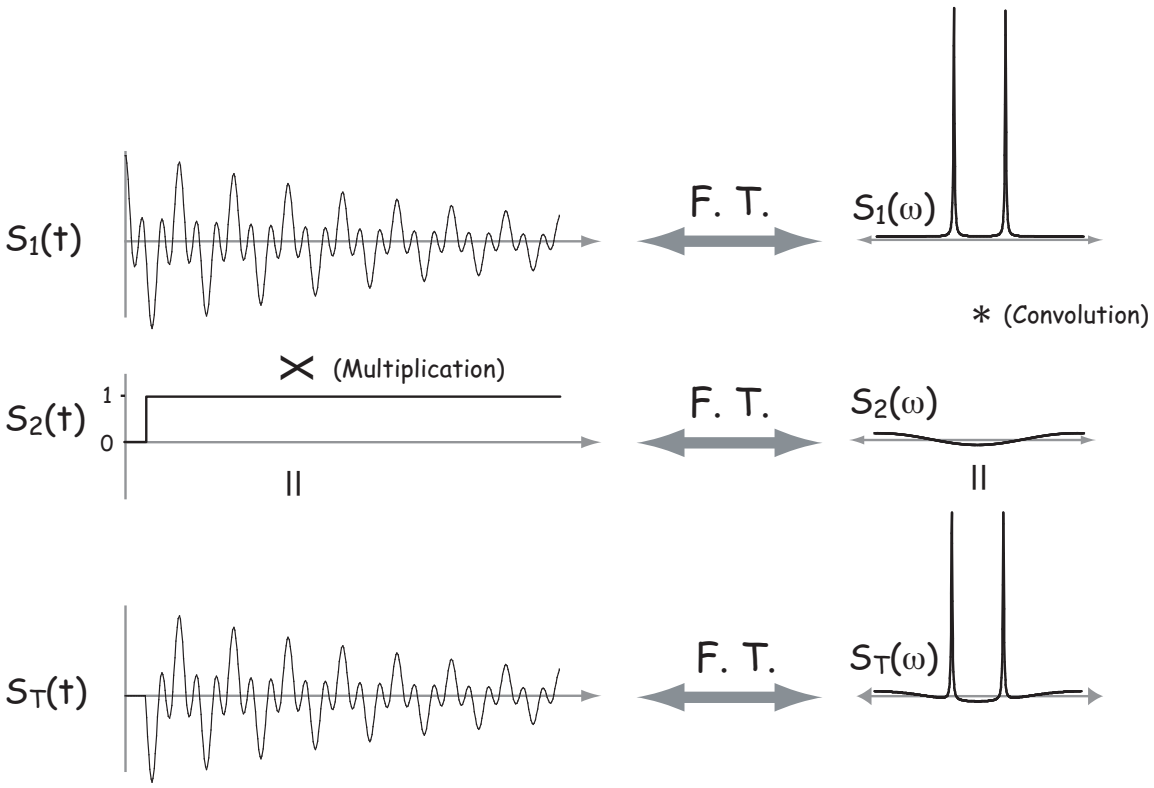

Here's an algorithm for phasing a spectrum containing multiple resonances. Take, for example, the unphased spectrum below.

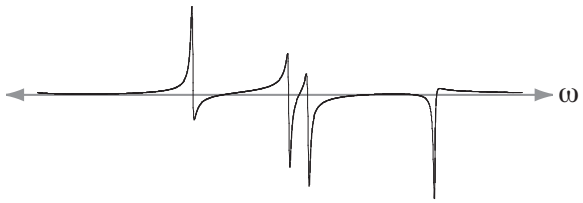

Apply zeroth order phase correction until one peak is completely absorption mode lineshape.

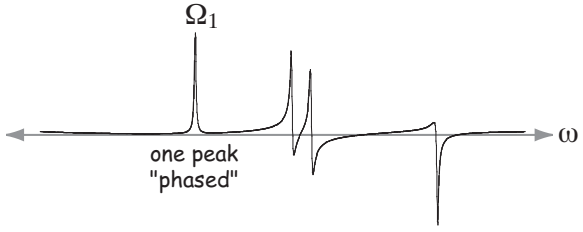

P. J. Grandinetti, November 23, 2009

Since this peak (at Ω_1) should look the same when the whole spectrum is phased, then we know any further phase corrections should not affect this peak. To force this constraint we set

$$\phi(\Omega_1) = \phi_0 + \Omega_1 t_0 = 0.$$

With this equation we can solve for ϕ_0 obtaining

$$\phi_0 = -\Omega_1 t_0,$$

and substituting this expression back into Eq. (1.34) we obtain

$$\phi(\omega) = (\omega - \Omega_1)t_0. \tag{1.37}$$

Now the only adjustable variable is t_0, and we can vary it until all the peaks are pure absorption mode.

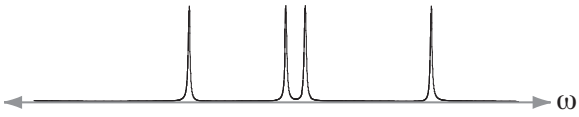

In this approach, Ω_1 is sometimes called the "pivot" frequency.

1.7 Inhomogeneous External Magnetic Fields and T_2^*

So far we have assumed that the external magnetic field was the same for all spins throughout the sample. In practice, however, there will be some spatial variations in the external magnetic field strength across the sample. Let's consider the effect of an inhomogeneous external magnetic field on our NMR spectrum.

A spatial variation in the external magnetic field makes the precession frequency depend on position in sample, that is

$$\omega_0(\mathbf{r}) = \gamma(1-\sigma)B_0(\mathbf{r}).$$

The total signal in the rotating frame becomes an integral over the volume of the sample,

$$S_{\text{total}}(t) = \int\int\int \rho(\mathbf{r}) e^{i\Omega(\mathbf{r})t} \cdot e^{-t/T_2} dV,$$

where $\rho(\mathbf{r})$ is the density of nuclei at $\mathbf{r}$. Even without knowing the functional form of the spatial variation in magnetic field and thus frequency, it is easily concluded that the decay of the total signal will be faster in an inhomogeneous field compared to a homogeneous field. For example, if there is a distribution of frequency clearly at long times the individual signal oscillations will be out of phase and thus will be destructively interfering at long times. Whereas at short times the oscillations from different signal will still be relatively in phase and will add up more constructively than at later times. The Fourier transform of a time domain signal from a sample in an inhomogeneous magnetic field will appear wider than the signal of a sample in a homogeneous field. Without knowing the functional form for the spatial field variations, it is impossible to predict the absorption mode lineshapes. Thus in the presence of an inhomogeneous magnetic field the full width at half height, Γ, can not longer be simply related to T_2, i.e., $\Gamma \neq 2/T_2$.

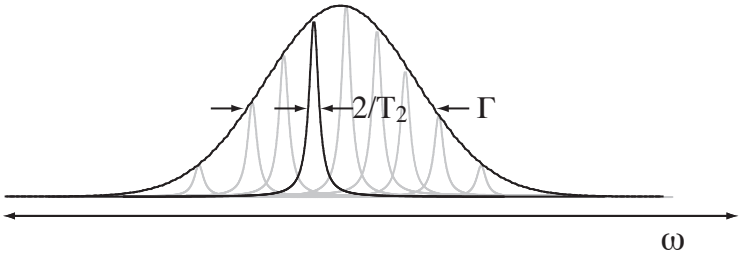

Often times, NMR spectroscopists will measure the full width at half height of an inhomogeneous broadened lineshape and use this number to report a quantity called T_2^*, defined as

$$T_2^* = 2/\Gamma.$$

One should not conclude, however, that a reported T_2^* means that lineshape is Lorentzian.

1.8 Limitations of the Bloch Equations

1.8.1 Nuclei with Electric Quadrupole Moments

We have seen that a nucleus with a non-zero angular momentum possesses a magnetic dipole moment vector. For the ^{1}H isotope, which only contains a single proton of spin $I = 1/2$, the nucleus only has the three internal degrees of freedom associated with the three components of its magnetic dipole moment vector. The Bloch equations were designed to describe an ensemble of such spin 1/2 nuclei, each having only three internal degrees of freedom.

In heavier isotopes and elements, the nucleus of the atom will contain additional protons and neutrons, and with them a corresponding increase in the available degrees of freedom for the nucleus. Although neutrons have no charge, they do have a spin angular momentum and a magnetic moment. With an increase in the number of nucleons we will find additional degrees of freedom within the nucleus that can be manipulated in the NMR experiment. These additional degrees of freedom can be described in terms of higher order magnetic and electric multipole moments. Due to symmetry restrictions only certain magnetic and electric multiple moments are allowed as a function of total angular momentum. The allowed moments up to $l = 4$ (hexadecapole) are summarized below for isotopes with total angular momentum up to $I = 2$.

Nuclear Spin	$l = 0$ monopole	$l = 1$ dipole	$l = 2$ quadrupole	$l = 3$ octapole	$l = 4$ hexadecapole
$I = 0$	electric	0	0	0	0
$I = \frac{1}{2}$	electric	magnetic	0	0	0
$I = 1$	electric	magnetic	electric	0	0
$I = \frac{3}{2}$	electric	magnetic	electric	magnetic	0
$I = 2$	electric	magnetic	electric	magnetic	electric

Every multipole moment, l, will bring $2l + 1$ additional degrees of freedom to the nucleus in the NMR experiment. The Bloch equations, designed to describe an ensemble of uncoupled spin 1/2 nuclei, are inadequate for uncoupled nuclei with spin $I > 1/2$, that is, with more than three degrees of freedom. It is possible to modify the Bloch Equations to describe this higher dimensional motion, but this motion is just as easily described using the well-established machinery of quantum mechanics. In later chapters, we will look in detail at how quantum mechanics describe the NMR experiment.

It is also useful to note that just as the nuclear magnetic dipole moment interacts with external magnetic fields, the nuclear electric quadrupole moment interacts with external electric fields, or more

specifically, surrounding electric field gradients. These electric field gradients are generated by orbiting electrons as well as neighboring nuclei. Additionally, just as the vector elements of the nuclear magnetic dipole moment precess in an externally applied magnetic field, the tensor elements of the nuclear electric quadrupole moment will precess in an external electric field gradient[7]. Measuring the frequencies of these oscillations allows us to measure the electric field gradient surrounding a nucleus, which in turn provides information about the local geometry and bonding around that atom.

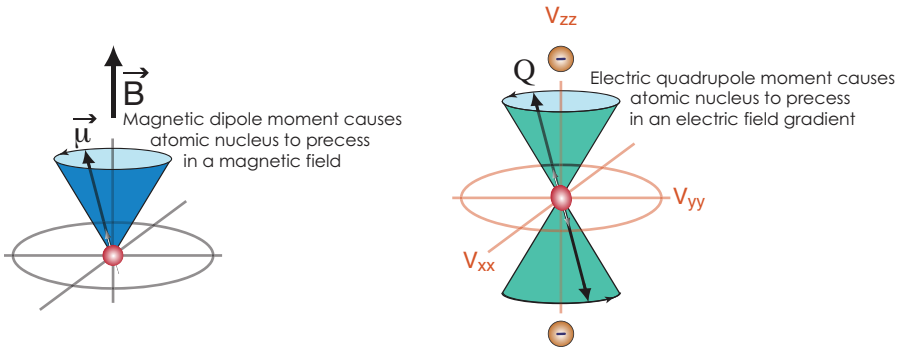

In principle, there will be couplings between the higher nuclear multipole moments and surrounding electric and magnetic fields, but in practice, attempts to measure such couplings have been inconclusive [3].

1.8.2 Coupling between distinguishable nuclei

So far in our discussion we have only considered isolated nuclei interacting with external magnetic and electric fields. In samples containing nuclei with abundant NMR active isotopes there will also be interactions between nuclear magnetic moments.

1.8.2.1 Magnetic Dipole Coupling between Nuclei

The classical interaction energy between two magnetic moments $\boldsymbol{\mu}_1$ and $\boldsymbol{\mu}_2$ is given by

$$E = \frac{\boldsymbol{\mu}_1 \cdot \boldsymbol{\mu}_2}{r^3} - \frac{3(\boldsymbol{\mu}_1 \cdot \mathbf{r})(\boldsymbol{\mu}_2 \cdot \mathbf{r})}{r^5},$$

[7]One might wonder if it is possible to directly detect the oscillations in the electric quadrupole moment tensor elements with a quadrupole condensor and measure the distribution of electric field gradients experienced by the nuclei in the sample. Although such experiments have been suggested [2], the direct measurement of the oscillations of the nuclear electric quadrupole moment are much less sensitive than the indirect measurement of their oscillations with NMR through their effect on the magnetic dipole vector oscillations.

and where the **r** is the internuclear vector, and $\boldsymbol{\mu}_1$ and $\boldsymbol{\mu}_2$ are the vectors describing the direction of each magnetic moment.

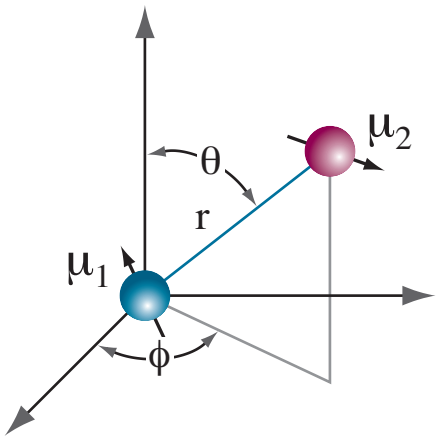

1.8.2.2 Indirect J Coupling between Nuclei

In addition to the direct dipolar coupling between nuclei there will also be an indirect J coupling between nuclei. The mechanism behind J coupling is more theoretically involved than the dipolar coupling. Qualitatively, we can think of J coupling as a two step process. First, the magnetic moments of valence electrons orbiting nucleus A get polarized in the same direction as the A nucleus' magnetic dipole moment. The polarized valence electrons then move to nucleus B, producing a small magnetic field that shifts the resonance frequency of nucleus B. The same process occurs in reverse, and in this manner, A and B become indirectly coupled.

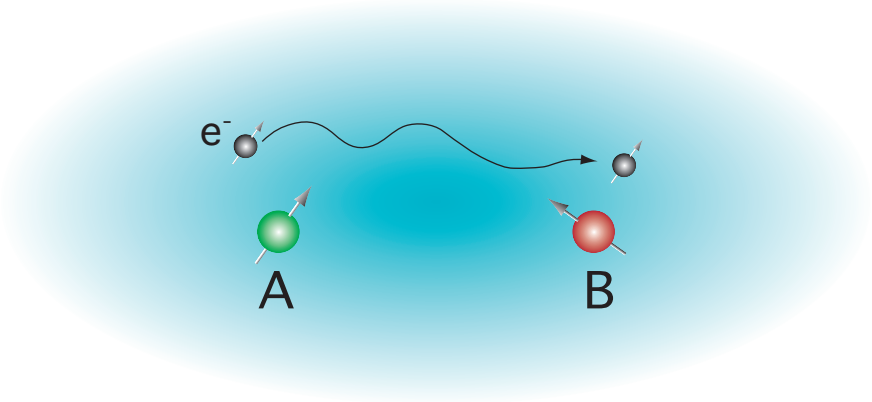

In either case, the total magnetic field experienced by a nucleus will vary depending on the spin state of neighboring nuclei. In such a situation we again find that the Bloch equations are inadequate for

coupled nuclei because they have more than three degrees of freedom. Additionally, the direct dipole-dipole and the indirect J coupling depend on the orientation of the internuclear vector and bonding orbitals, respectively. In the liquid and gas state this orientation dependence is averaged away by rapid molecular reorientations. Direct dipole-dipole couplings average to zero in liquids, whereas J couplings average to a non-zero scalar value.

1.9 Measuring Relaxation Times

Since NMR relaxation arises from the fluctuating fields produced by molecular motion, it is possible to use NMR relaxation times to characterize and quantify this motion. In this section we will examine two common approaches for measuring the spin-lattice relaxation time, T_1, introduced with the phenomenological Bloch Equations. It is important to note, however, that the Bloch equation's assumption of a single exponential recovery time is not valid for nuclei that have any time independent couplings, as described in the last section. That is, the Bloch Equations assume that all couplings, such as the quadrupolar, dipolar, and J coupling, are averaged to zero by molecular motion, or selective rf irradiation (*i.e.*, spin decoupling). If this is not true, multi-exponential recoveries can occur and a single exponential recovery time, *i.e.,* T_1, would no longer be appropriate. The problem is still tractable, but a more detailed analysis of the data is required, often combined with other experiments, and will not be described in this section. If your main goal is to obtain a proper value for the equilibration time so that the signal-to-noise ratio is acceptable and the integrated intensities are quantitative then it is not a problem if your recovery is not exponential. Performing the saturation or inversion recovery experiment described below is sufficient to determine the equilibration time needed for all the magnetization to recover, *i.e.*, $\sim 99\%$ of M_{eq}.

1.9.1 Spin-Lattice Relaxation Times

In this section, we will assume the nuclei relax with single exponential recoveries, and describe two experiments for measuring the spin-lattice relaxation time T_1: the saturation recovery method and the inversion recovery method.

1.9.1.1 The Saturation Recovery Experiment

In the saturation recovery experiment the magnetization is rotated from z to the x-y plane and allowed to completely dephase during a period τ that is set to approximately 2 or 3 times T_2. This process is repeated many times so there exists no net magnetization in any direction, and the magnetization is saturated. During the time t_1 the magnetization recovers, growing along the z-axis. This recovery is monitored by applying a $\pi/2$ pulse after t_1 and measuring the signal intensity.

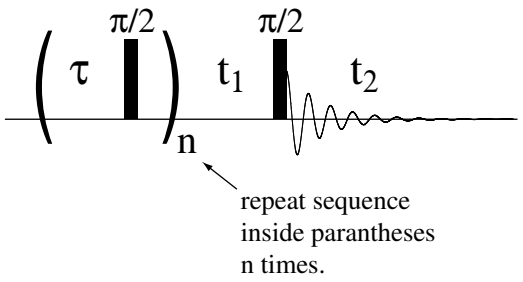

From the Bloch equations we know the z-component of the magnetization will recover according to

$$M_z(t) = M_{eq}(1 - e^{-t_1/T_1}) + M_z(0)e^{-t_1/T_1}.$$

Inserting the initial condition created by the saturation pulse train, $M_z(0) = 0$, into this expression we obtain

$$M_z(t_1) = M_{eq}(1 - e^{-t_1/T_1}).$$

Below is a plot of the percent recovery of the longitudinal (M_z) magnetization as a function of t_1 given in multiples of T_1.

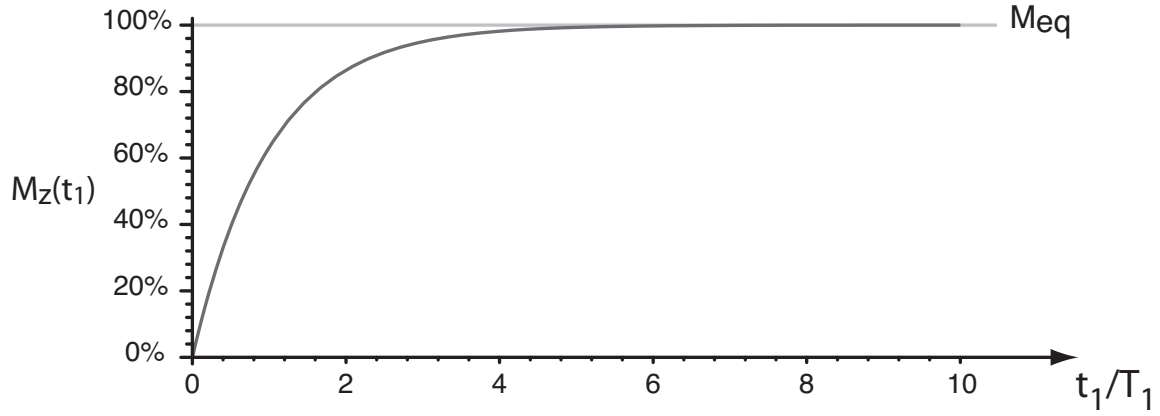

At $t_1 = 0$ we have $M_z(0) = 0$ and at $t_1 = \infty$ we have $M_z(\infty) = M_{eq}$. The saturation recovery experiment provides a less precise measurement of T_1 than the inversion recovery experiment, described in the next section. Unlike the inversion recovery experiment, however, the saturation recovery experiment doesn't require an equilibration time, and for samples with long T_1 values (greater than 30 seconds) this can lead to significant shorter experiment times.

P. J. Grandinetti, November 23, 2009

1.9.1.2 The Inversion Recovery Experiment

In the inversion recovery experiment the magnetization is rotated from the $+z$ axis to the $-z$ axis. The magnetization recovers and grow back towards the $+z$ axis during a t_1 period. The recovery of the magnetization is monitored by applying a $\pi/2$ pulse after t_1 and measuring the signal intensity.

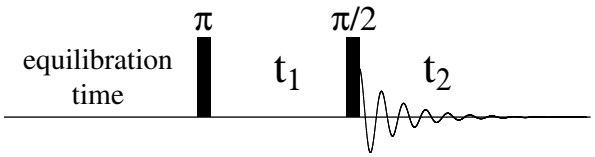

Again, using the Bloch equations we have

$$M_z(t) = M_{eq}(1 - e^{-t_1/T_1}) + M_z(0)e^{-t_1/T_1}.$$

Here we have $M_z(0) = -M_{eq}$ so

$$M_z(t) = M_{eq}(1 - 2e^{-t_1/T_1}).$$

Below is a plot of the percent recovery of the longitudinal (M_z) magnetization as a function of t_1 given in multiples of T_1.

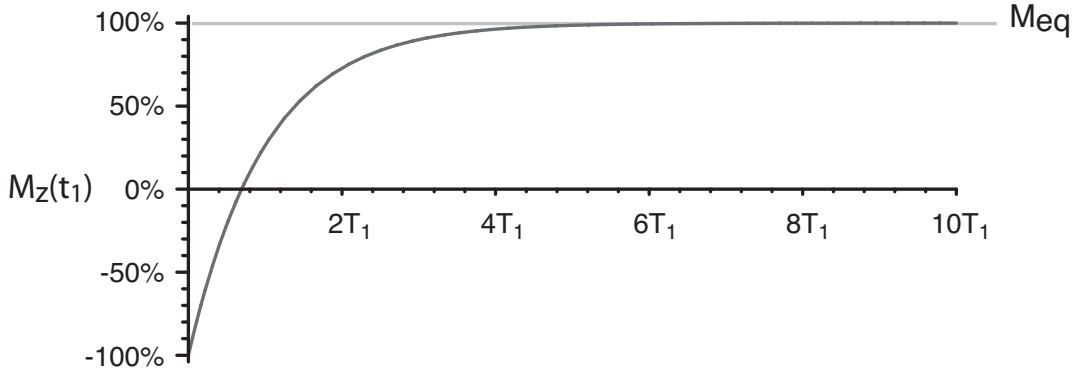

At $t_1 = 5T_1$ then $M_z(5T_1) = 0.993M_{eq}$. The inversion recovery experiment has a wider range of signal variation that makes it more precise. A quick approach for estimating T_1 is to locate the time $t_1 = \tau$ when $M_z(\tau) = 0$. One can then show that $T_1 = \tau/\ln 2$. The disadvantage of the Inversion Recovery sequence is that you need an equilibration time of a least five times the longest T_1. Since you don't know T_1 then you have to guess, and this makes the process somewhat iterative.

P. J. Grandinetti, November 23, 2009

1.9.2 Spin-Spin Relaxation Times

In theory one can obtain T_2 by taking half the inverse of the full width at half height in Hertz of a resonance in an NMR spectrum. Unfortunately, the line widths of resonances in NMR are often dominated by the inhomogeneities in the magnetic field rather than T_2.

1.9.2.1 The Spin Echo Experiment

It turns out that in many systems it is possible to measure the true T_2 even in the presence of inhomogeneous broadening. One approach is to apply a second rf pulse before detecting the signal. Consider the following sequence

$$\text{equilibrate} - (\pi/2)_x - t_1 - (\pi)_x - t_2 \longrightarrow$$

How is the signal detected during t_2 affected by this two pulse sequence? Let's examine the path of the magnetization vector under this sequence of events. To simplify our discussion, we will assume that $t_1 + t_2 \ll T_1$, and neglect spin-lattice relaxation. The evolution of the magnetization during this experiment will go as follows:

$$\mathbf{M} = \underbrace{M_{eq}}_{M_0}\,\mathbf{e}^0.$$

$$\Big\downarrow (\pi/2)_x$$

$$\mathbf{M}^\dagger = \underbrace{\frac{i}{\sqrt{2}}M_{eq}}_{M^\dagger_{+1}}\,\mathbf{e}^{+1} \underbrace{+\frac{i}{\sqrt{2}}M_{eq}}_{M^\dagger_{-1}}\,\mathbf{e}^{-1}$$

$$\Big\downarrow t_1 \text{ evolution}$$

$$\mathbf{M}(t_1) = \underbrace{\frac{i}{\sqrt{2}}M_{eq}e^{i\Omega(\mathbf{r})t_1}\cdot e^{-t_1/T_2}}_{M_{+1}(t_1)}\,\mathbf{e}^{+1} \underbrace{+\frac{i}{\sqrt{2}}M_{eq}e^{-i\Omega(\mathbf{r})t_1}\cdot e^{-t_1/T_2}}_{M_{-1}(t_1)}\,\mathbf{e}^{-1}$$

$$\Big\downarrow (\pi)_x$$

$$\mathbf{M}(t_1)^\dagger = \underbrace{\frac{i}{\sqrt{2}}M_{eq}e^{-i\Omega(\mathbf{r})t_1}\cdot e^{-t_1/T_2}}_{M_{+1}(t_1)^\dagger}\,\mathbf{e}^{+1} + \underbrace{\frac{i}{\sqrt{2}}M_{eq}e^{i\Omega(\mathbf{r})t_1}\cdot e^{-t_1/T_2}}_{M_{-1}(t_1)^\dagger}\,\mathbf{e}^{-1}.$$

$$\Big\downarrow t_2 \text{ evolution}$$

$$\mathbf{M}(t_1,t_2) = \underbrace{\frac{i}{\sqrt{2}}M_{eq}e^{-i\Omega(\mathbf{r})(t_1-t_2)}\cdot e^{-(t_1+t_2)/T_2}}_{M_{+1}(t_1,t_2)}\,\mathbf{e}^{+1} + \underbrace{\frac{i}{\sqrt{2}}M_{eq}e^{i\Omega(\mathbf{r})(t_1-t_2)}\cdot e^{-(t_1+t_2)/T_2}}_{M_{-1}(t_1,t_2)}\,\mathbf{e}^{-1}.$$

P. J. Grandinetti, November 23, 2009

Notice that the effect of the $(\pi)_x$ pulse is to swap the M_{+1} and M_{-1} coherences. Focusing on the transverse magnetization we see that when $t_1 = t_2 = \tau$ we get the remarkable result

$$\mathbf{M}(\tau) = \underbrace{\frac{i}{\sqrt{2}} M_{eq} e^{-2\tau/T_2}}_{M_{+1}(\tau)} \mathbf{e}^{+1} + \underbrace{\frac{i}{\sqrt{2}} M_{eq} e^{-2\tau/T_2}}_{M_{-1}(\tau)} \mathbf{e}^{-1}.$$

When both t_1 and t_2 are increased while keeping $t_1 = t_2$, the evolution of the signal will be independent of $\Omega(\mathbf{r})$. In this two pulse experiment on samples with large inhomogeneous line broadenings the signal can even appear dead after the $\pi/2$ pulse but after a π pulse the signal returns in what is called a spin echo[8].

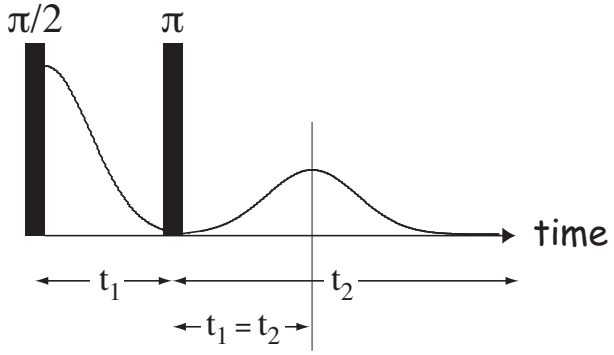

That is, independent of the frequencies $\Omega(\mathbf{r})$ present, the magnetization vectors for all sites return to the starting point (the y axis) when $t_1 = t_2$. The only decay of the echo top (refocussed magnetization) is due to T_2 relaxation. This sequence gives us a method of measuring T_2 in the presence of field inhomogeneities.

The spin echo arises in many other contexts in NMR, and will be a key concept in understanding numerous multi-dimensional NMR experiments. A popular analogy for the spin echo experiment is to consider a group of runners lined up at the starting line of a circular track. When the whistle is blown (the $\pi/2$ pulse), the runners begin running at various speeds depending on their abilities. After a time t_1, the whistle is blown again (the π pulse) and the runners all stop and run in the opposite direction. At a time $t_2 = t_1$ after the second whistle the runners, if they ran at the same speed in both directions, will all pass the starting line simultaneously as they continue running in the opposite direction. This lining up of the runners as they pass the starting line is analogous to what happens to the magnetization in the spin echo experiment.

[8]Sometimes called the Hahn spin echo, after its discover Erwin Hahn.

There are two possible complications with measuring T_2 values with the spin echo experiment. The first occurs for nuclei experiencing homonuclear J-couplings. Here, the echo tops are modulated as a function of t_1 due to evolution under the J-coupling. This evolution cannot be refocused by the π pulse. The second complication arises from molecular diffusion. If a molecule diffuse from one region of the sample to the next in a field gradient, then it may have different resonance frequencies during t_1 and t_2. Here there will be an incomplete refocusing of the echo.

1.9.2.2 Carr-Purcell Meiboom-Gill sequence

Carr and Purcell proposed a multiple echo sequence to minimize the effects of translational diffusion when measuring T_2, which, as modified by Meiboom and Gill and shown below, is commonly called the CPMG sequence.

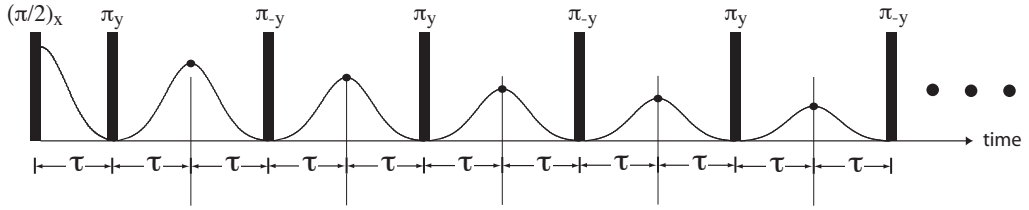

1.10 Coherence Transfer Pathways

Consider the two pulse NMR experiment shown below.

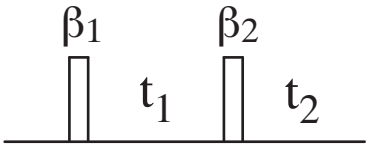

Is this the Spin Echo experiment of section 1.9.2, or the T_1 inversion recovery experiment of section 1.9.1.2? You might say it depends on the rotation angle used for the two pulses. That is, the spin echo experiment uses a $\pi/2$ and a π for the first and second pulse, respectively, whereas, the T_1 inversion recovery experiment uses a π and a $\pi/2$, respectively. In a sense, that is correct. But what if both pulses were $2\pi/3$ rotations? Would we observe a spin echo signal, an inversion recovery signal, or both? The answer is that we would observe both. This illustrates a common problem in multiple pulse NMR spectroscopy. There can be many different types of signals associated with the same pulse sequence, some desired and some undesired. To separate desired from undesired signals it is first necessary to understand how different signals originate from the same pulse sequence.

Consider the spin echo experiment. If we followed the path of the magnetization vector component responsible for the spin echo signal through the sequence we find that it starts out along the $\mathbf{e}^0$ direction, moves to the $\mathbf{e}^{-1}$ direction during t_1, and then to the $\mathbf{e}^{+1}$ direction during t_2 where it is detected. This "pathway" is different from the one associated with the inversion recovery pathway, where the detected magnetization vector component follows the path $\mathbf{e}^0 \rightarrow \mathbf{e}^0 \rightarrow \mathbf{e}^{+1}$. Note that the magnetization vector components only change direction during a pulse, and, as we saw in Eq. (1.5.1), during free evolution their directions remain unchanged.

If we wrote out all magnetization vector pathways possible in the two pulse experiment for arbitrary pulse lengths the resulting expansion would quickly become complicated. As you can see below, with each pulse the number of terms in the expansion grows exponentially.

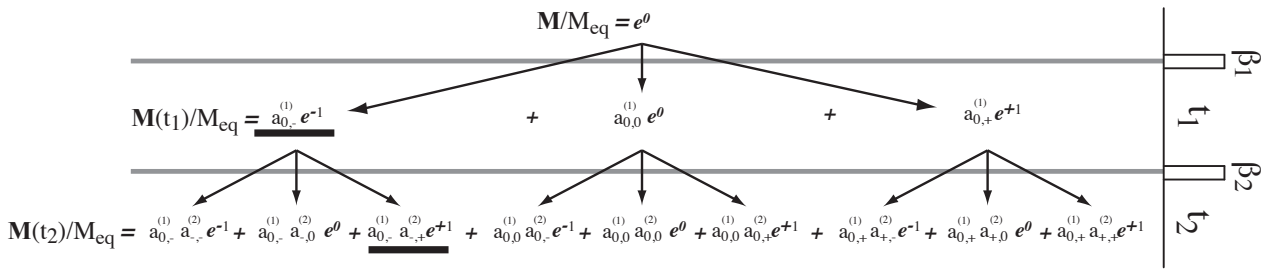

P. J. Grandinetti, November 23, 2009

After two pulses there will be 9 different terms contributing to the total magnetization, each multiplied by coefficients that carry the history of each term. Tracing the origins of each of these terms back to the initial magnetization along $\mathbf{e}^0$ also reveals all the possible transition frequency modulations that can be present in a signal. These possibilities can be graphically represented in what is called a **coherence transfer pathway**.

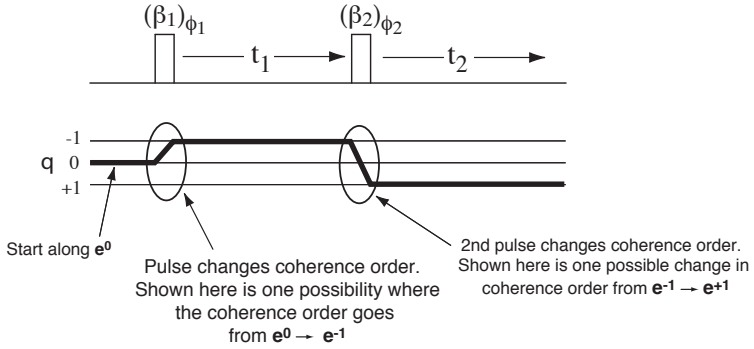

This pathway is associated with the underlined terms in our two magnetization vector expansion. For the two pulse sequence on a spin 1/2 there are eight other such "pathways". Below are examples of three others.

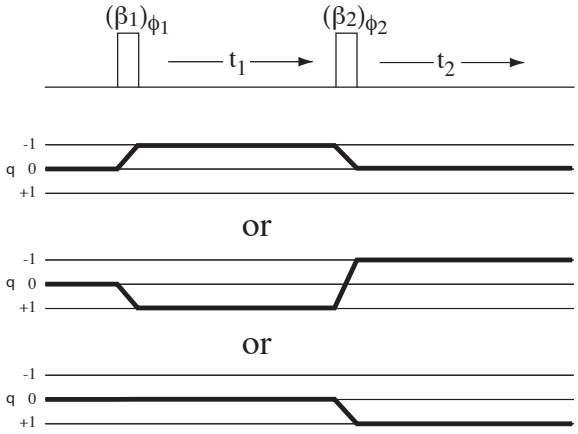

It is left as an exercise for the reader to draw the remaining pathways. The signals associated with each of the nine different pathways are not all unique. A pathway can give rise to a signal that is the complex conjugate of another. These complex conjugate pathways are easily identified since they will be mirror images of each other about the $q = 0$ coherence level. For example, the two pathways below are mirror images of each other about the $q = 0$ coherence level and therefore represent signals that will be complex conjugates of each other.

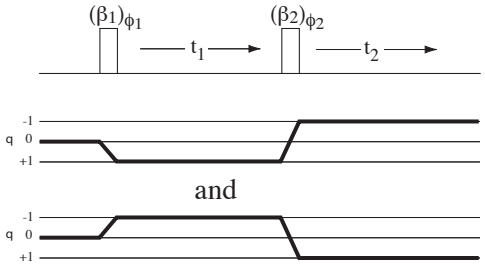

If you remove the redundancy of mirror image pathways, then the number of pathways that give rise to unique signals in a two pulse sequence on a spin 1/2 system is five. If we consider only those that end on the $q = +1$ coherence level, that is, assume that our receiver is a perfect detector of the observable M_+, then we only need to consider three pathways. Before we consider these three pathways, we note that, for reasons related to the quantum mechanical treatment of NMR the convention in NMR is to draw the mirror image (or complex conjugate) pathway with the coherence levels labeled as p, where $p = -q$. With that in mind, let's now consider the three pathways below.

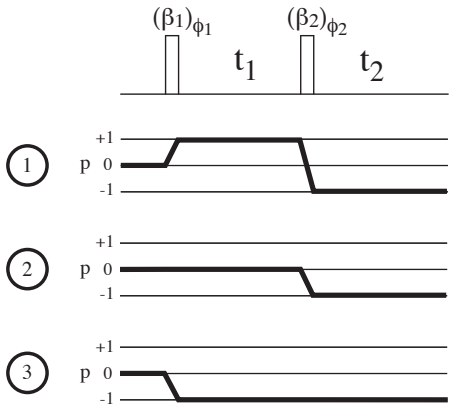

Each of these pathways describe a different NMR signal. For example, the Spin Echo experiment is described by pathway 1. Assuming that the absolute frequency associated with the $p = \pm 1$ coherence levels doesn't change between t_1 and t_2, then the change in the sign of the coherence level from $p = -1$ in t_1 to $p = +1$ in t_2 will lead to an echo formation during t_2 when $t_2 = t_1$. Similarly, the inversion-recovery T_1 measurement experiment is described by pathway 2. The Anti-Echo experiment is described by pathway 3. It has this name because when $t_1 = 0$ the Anti-Echo pathway signal in t_2, like the Echo pathway signal, contains only the right half of a spin echo signal, and with increasing t_1 the anti-echo signal maximum moves backwards in t_2, occurring "virtually" at the negative times $t_2 = -t_1$, where it cannot be detected.

P. J. Grandinetti, November 23, 2009

Let's consider the pathways for the two other experiments we've discussed so far, the saturation recovery and the CPMG sequences. In the saturation recovery experiment we have

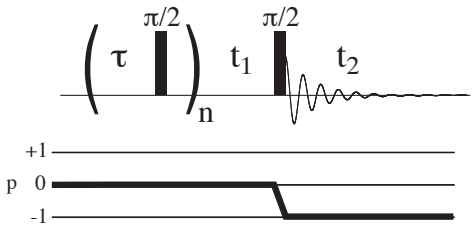

During the train of n pulses we intend to saturate the magnetization, and desire no coherence transfer at all. Thus we write the pathway during the pulse train to reflect no change in the coherence order[9] During the recovery time, t_1, there will be recovery along the z axis, which we will measure with the final $\pi/2$ pulse. The goal of the final $\pi/2$ pulse is to convert the M_0 ($p = 0$) order into an M_+ ($p = -1$) coherence that we can detect with our receiver coil.

In the CPMG experiment there will be two pathways from which we will acquire signal. The signal acquired from sequential echo tops will alternate between the two pathways shown below.

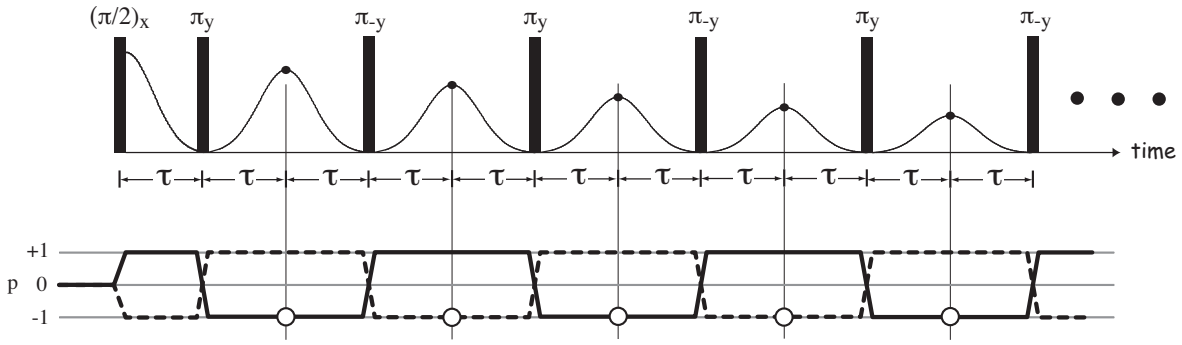

Because the two pathways are mirror images their signals will be complex conjugates of each other. Although signal from a given pathway will be missing every other point, the signal from a single pathway with all points can be reconstructed by combining the signal of one pathway with the complex conjugate of the other pathway.

An ensemble of coupled spin 1/2 nuclei, or an ensemble of uncoupled nuclei with spin $I > 1/2$, will have additional degrees of freedom that can be manipulated in the NMR experiment. These additional degrees of freedom are represented in coherence transfer pathways as coherence orders beyond $p = \pm 1$.

[9]Technically, one might argue that there is no magnetization along $\mathbf{e}_0$ direction after the pulse n pulses, when $t_1 = 0$, since the magnetization is saturated. That is correct. For practical purposes, however, we group this saturated state with the $\mathbf{e}_0$ magnetization components.

For example, a single spin I will have coherence orders extending over $-2I \leq p \leq 2I$. Generally, N coupled spins will have coherence orders extending over $-2L \leq p \leq 2L$, where $L = \sum_k I_k$.

1.11 Measuring Translational Diffusion Coefficients

The dependence of the echo intensity on molecular diffusion can be exploited as a means to measure translational diffusion coefficients [4, 5]. By applying linear magnetic field gradient,

$$\mathbf{B}(\mathbf{r}) = \mathbf{B}_0 + \mathbf{G} \cdot \mathbf{r},$$

across the sample and performing the spin echo experiment one can solve the modified Bloch equation,

$$\frac{d\mathbf{M}(\mathbf{r})}{dt} = \gamma' \mathbf{M}(\mathbf{r}) \times \mathbf{B}(\mathbf{r}, t) - [\mathbf{R}]\{\mathbf{M}(\mathbf{r}) - \mathbf{M}_{eq}\} + D\nabla^2 \mathbf{M}(\mathbf{r}). \tag{1.38}$$

to obtain an analytical expression for the echo intensity, given by

$$S(\tau, G) = S(0, 0) \exp\left(-\frac{2}{3} D\gamma^2 G^2 \tau^3 - 2\tau/T_2\right). \tag{1.39}$$

By applying a systematic variation in magnetic field gradient strength, G, as well as the echo dephasing time, τ, one can measure both the diffusion coefficient, D, and spin-spin relaxation time, T_2.

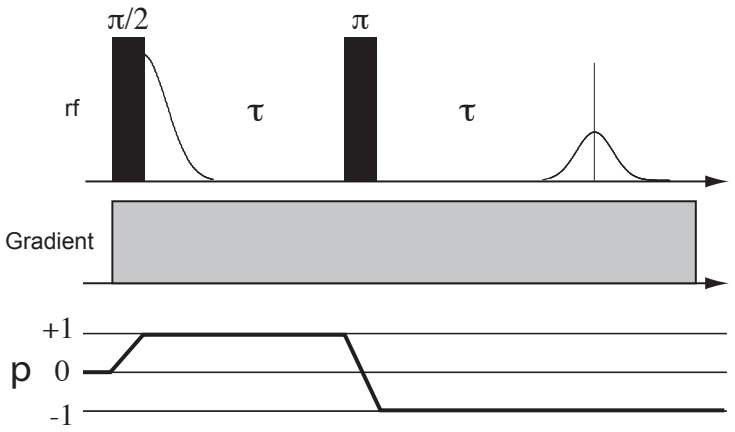

1.11.1 Pulsed Field Gradients

A more robust method for measuring diffusion coefficients employs pulsed field gradients [6] instead of a static field gradient. In this approach, as illustrated below, the gradient is pulsed on before and after the π pulse, each time for a duration of δ.

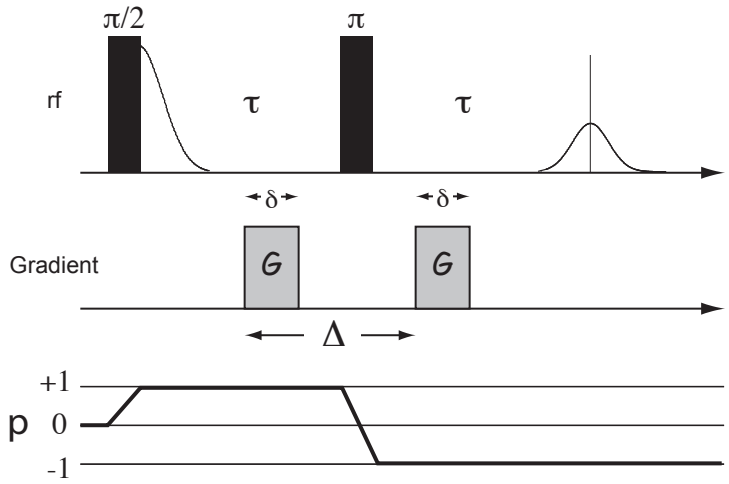

The analytical expression for the echo intensity is given by

$$S(\tau, G) = S(0,0)\exp\Big(-\gamma^2 G^2 \delta^2 D(\Delta - \delta/3) - 2\tau/T_2\Big), \tag{1.40}$$

where Δ is the time between the two gradient pulses. Since the detection of the echo signal occurs in a relatively homogeneous magnetic field a high resolution spectrum with higher sensitivity is obtained. This is particularly advantageous for making simultaneous measurements of diffusion coefficients in samples containing mixtures of molecules. Additionally, the experimenter has the additional option of varying the gradient pulse duration, δ, gradient pulse interval, Δ, or gradient strength, G, when measuring the diffusion coefficient. A plot of $\log[S(2\tau)/S(0)]$ versus $\delta^2(\Delta - \delta/3)G^2$ should yield a straight line passing through the origin with a slope of $-0.4343\gamma^2 D$. With pulsed field gradients, values of D as low as 10^{-9} cm^2 sec^{-1} can be measured. This is about two orders of magnitude slower than D values measurable with static field gradients.

It is also possible, with this sequence, to measure flow: a coherent motion of all molecules with a uniform velocity vector $\mathbf{v}$. The effect of flow is to cause a phase modulation of the echo tops. Combined with the attenuation of the echo tops due to diffusion the analytical expression for the echo intensity is given by

$$S(\tau, G) = S(0)\exp\Big(i\gamma\delta\mathbf{G}\cdot\mathbf{v}\Delta - (\gamma G\delta)^2 D(\Delta - \delta/3) - 2\tau/T_2\Big). \tag{1.41}$$

Finally, recall that the CPMG sequence can be used to minimize the effects of translational diffusion (and flow) when measuring T_2. In the presence of a gradient the CPMG echo intensities will be given by

$$S(t = 2n\tau) = S(0)\exp\Big(-\frac{1}{3}\gamma^2 G^2 \tau^2 D t - t/T_2\Big). \tag{1.42}$$

By reducing the time, τ, between π pulses, the effect of the diffusion can be minimized, and the T_2 can be measured more reliably.

1.12 Interpreting Relaxation Times

Constructing a theoretical model to interprete NMR relaxation times can be relatively simple or completely intractable, depending on the sample. The general approach starts with determining which fluctuating couplings contribute to the relaxation process. For spin 1/2 nuclei these couplings typically arise from magnetic dipole interactions, whereas for spin $I > 1/2$ they can arise from electric quadrupole as well as magnetic dipole interactions. For each of these possibilities we can obtain an expression for the relaxation times, and the overall spin relaxation rates will be the sum from all the contributions,

$$\frac{1}{T_1} = \left(\frac{1}{T_1}\right)_{paramagnetic} + \left(\frac{1}{T_1}\right)_{quadrupole} + \left(\frac{1}{T_1}\right)_{dipole} + \left(\frac{1}{T_1}\right)_{chem.shift} + \cdots. \tag{1.43}$$

Like resistors in parallel, we see that relaxation can easily be dominated by one coupling that is larger than the rest. Typically, the relaxation is dominated by fluctuating unpaired electron-nuclear dipolar couplings, followed by quadrupolar couplings, dipolar couplings, and chemical shift anisotropy. Also important is whether the fluctuating couplings experienced by a nucleus are coming from other nuclei or electrons in the same molecule (intramolecular couplings) or other molecules (intermolecular couplings). Chemical shift and electric quadrupole couplings are generally intramolecular, whereas dipolar couplings can be intra- or inter-molecular.

1.12.1 Time Correlation and Spectral Density Functions

Fluctuations in couplings arise from fluctuations in the distances and orientations of atoms and molecules nearby the nucleus in question. Thus, we introduce the concept of a time correlation function to quantify the time scale on which these fluctuations occur. For example, the time correlation function for an intermolecular distance vector can be written

$$G(\tau) = \langle \mathbf{r}(t) \cdot \mathbf{r}(t+\tau) \rangle,$$

where the angle brackets represent an ensemble average. In the same manner one can imagine a time correlation function for a nuclear spin coupling, C, that depends on the same fluctuating internuclear vector,

$$G_C(\tau) = \langle C(\mathbf{r}(t))\, C(\mathbf{r}(t+\tau)) \rangle,$$

which we more simply write as

$$G_C(\tau) = \langle C(t)\, C(t+\tau) \rangle.$$

We can also write the time-correlation function of two different couplings,

$$G_{CD}(\tau) = \langle C(t)\, D(t+\tau)\rangle.$$

This is called a cross-correlation function, whereas $G_C(\tau)$ is called an auto-correlation function.

The spectral density function is the Fourier transform of the time correlation function,

$$J(\omega) = \int_0^\infty G(\tau) e^{-i\omega\tau} d\tau$$

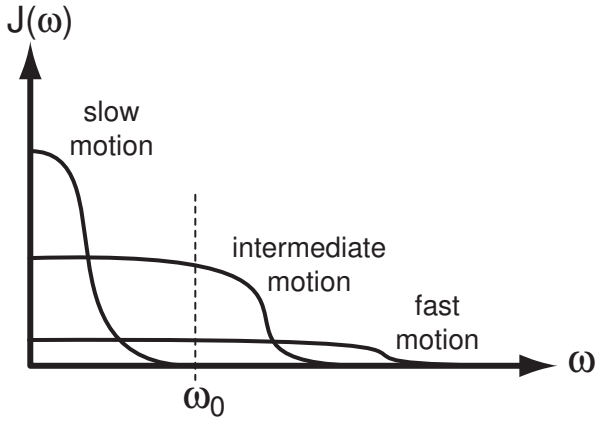

One of the simplest models is that of random isotropic molecular tumbling where

$$G(\tau) = G(0) e^{-|\tau|/\tau_c},$$

where τ_c is the reorientational correlation time for the molecular tumbling. The Stokes-Einstein-Debye relation predicts the reorientational correlation time as

$$\tau_c = \frac{\eta_s V}{kT}, \tag{1.44}$$

where η_s is the solvent viscosity and V the solvated volume of the rotating molecule. If we assume that the Stokes-Einstein-Debye relation holds, then the NMR relaxation times can be used to obtain information about molecular size or local viscosity. This equations also provides an understanding of why it is difficult to obtain high resolution solution-state NMR studies of molecules with large molecular weights. With increasing molecular size, there will be a corresponding increase in molecular reorientation times which in turn leads to decreased T_2, and excessive line broadenings.

1.12.2 Relaxation via Dipolar Couplings

To describe time correlation functions for translational and reorientation motion it is convenient to use the three functions

$$F_0(r,\theta,\phi) = \frac{1}{r^3}(1-3\cos^2\theta),$$

$$F_1(r,\theta,\phi) = \frac{1}{r^3}\sin\theta\cos\theta\exp(i\phi), \tag{1.45}$$

$$F_2(r,\theta,\phi) = \frac{1}{r^3}\sin^2\theta\exp(i2\phi),$$

which are related spherical harmonic functions, with the angles θ and ϕ and the distance r defined on page 36 for the dipolar coupling. Using these definitions we further define the time correlation and spectral density functions,

$$G_n(\tau) = \langle F_n(t)\,F_n(t+\tau)\rangle, \quad \text{and} \quad J_n(\omega) = \int_0^\infty G_n(\tau)e^{-i\omega\tau}d\tau. \tag{1.46}$$

One can further show that the spectral density functions with different n are all related to a single function $j(\omega)$, called the reduced spectral density function, according to

$$b^2\,j(\omega) = \frac{15}{12}\,J_0(\omega) = \frac{15}{2}\,J_1(\omega) = \frac{15}{8}\,J_2(\omega), \tag{1.47}$$

where

$$b = -\frac{\mu_0\hbar\gamma_I\gamma_S}{4\pi r^3} \tag{1.48}$$

If we assume the spectral density function arises from a simple model of isotropic molecular tumbling, having a single reorientational correlation time τ_c, then $j(\omega)$ is given by

$$j(\omega) = \frac{2\tau_c}{(1+\omega^2\tau_c^2)}. \tag{1.49}$$

In the limit of extreme narrowing, $\omega_0\tau \ll 1$, we obtain

$$j(\omega) \approx 2\tau_c, \tag{1.50}$$

1.12.2.1 Nuclei with Identical Resonance Frequencies

When there is a dipolar coupling between two nuclei with the same angular momentum, I, and resonance frequency, ω_0, then the spin lattice relaxation arising from the modulation of the dipolar coupling is given by

$$\frac{d(M_{z_1}+M_{z_2})}{dt} = -\frac{1}{T_1}\left\{(M_{z_1}-M_{z_1}^{eq})+(M_{z_2}-M_{z_2}^{eq})\right\}, \tag{1.51}$$

where

$$\frac{1}{T_1} = \frac{I(I+1)\,b^2}{15}\left[3j(\omega_0) + 6j(2\omega_0)\right]. \tag{1.52}$$

Similarly, for the transverse component, we have

$$\frac{d(M_{+1_1} + M_{+1_2})}{dt} = -\frac{M_{+1_1} + M_{+1_2}}{T_2}, \tag{1.53}$$

where

$$\frac{1}{T_2} = I(I+1)\,b^2\left[\frac{3}{10}\,j(0) + \frac{1}{2}\,j(\omega_0) + \frac{3}{15}\,j(2\omega_0)\right]. \tag{1.54}$$

Finally, note that in the Motional Narrowing Regime we obtain

$$\frac{1}{T_1} \approx \frac{1}{T_2} \approx I(I+1)\,b^2\,2\,\tau_c. \tag{1.55}$$

1.12.2.2 Nuclei with Different Resonance Frequencies

When there is a magnetic dipolar coupling between two nuclei having different resonance frequencies, for example, a nucleus of spin I and a nucleus of spin S, the longitudinal recovery of the magnetization for I and S nuclei follows the coupled differential equations, also known as the Solomon equations:

$$\begin{aligned}
\frac{dM_{z_I}}{dt} &= -\frac{1}{T_1^{II}}(M_{z_I} - M_{z_I}^{eq}) - \frac{1}{T_1^{IS}}(M_{z_S} - M_{z_S}^{eq}), \\
\frac{dM_{z_S}}{dt} &= -\frac{1}{T_1^{SI}}(M_{z_I} - M_{z_I}^{eq}) - \frac{1}{T_1^{SS}}(M_{z_S} - M_{z_S}^{eq}),
\end{aligned} \tag{1.56}$$

where

$$\frac{1}{T_1^{II}} = \frac{S(S+1)\,b^2}{15}\left[j(\omega_I - \omega_S) + 3j(\omega_I) + 6j(\omega_I + \omega_S)\right], \tag{1.57}$$

and

$$\frac{1}{T_1^{IS}} = \frac{I(I+1)\,b^2}{15}\left[j(\omega_I - \omega_S) - 6j(\omega_I + \omega_S)\right]. \tag{1.58}$$

Expressions for T_1^{SS} and T_1^{SI} can be obtained from the expressions above by interchanging the indices I and S. The times T_1^{SS} and T_1^{II} are called auto-relaxation times, and T_1^{IS} and T_1^{SI} are called cross-relaxation times.

Similarly, for the M_I transverse component one finds

$$\frac{dM_{+1_I}}{dt} = -\frac{M_{+1_I}}{T_2}, \tag{1.59}$$

where

$$\frac{1}{T_2^I} = S(S+1)\,b^2\left[\frac{2}{15}\,j(0) + \frac{3}{15}\,j(\omega_S) + \frac{1}{10}\,j(\omega_I) + \frac{3}{15}\,j(\omega_I + \omega_S) + \frac{1}{30}\,j(\omega_I - \omega_S)\right]. \tag{1.60}$$

In the Motional Narrowing Regime If we assume the spectral density function arises from a simple model of isotropic molecular tumbling, having a single reorientational correlation time τ_c, then one can show that

$$\left(\frac{1}{T_1^{II}}\right) \Big/ \left(\frac{1}{T_1^{IS}}\right) \approx \frac{2S(S+1)}{I(I+1)}. \tag{1.61}$$

Thus, we define

$$m_{z_I} = \frac{M_{z_I}}{I(I+1)}, \quad \text{and} \quad m_{z_S} = \frac{M_{z_S}}{S(S+1)}, \tag{1.62}$$

and obtain

$$\frac{dm_{z_I}}{dt} \approx -\frac{1}{T_1^{II}}\left[(m_{z_I} - m_{z_I}^{eq}) - \frac{1}{2}(m_{z_S} - m_{z_S}^{eq})\right], \tag{1.63}$$

$$\frac{dm_{z_S}}{dt} \approx -\frac{1}{T_1^{SS}}\left[(m_{z_I} - m_{z_I}^{eq}) - \frac{1}{2}(m_{z_S} - m_{z_S}^{eq})\right]. \tag{1.64}$$

We still have two coupled differential equations but now the the cross-relaxation times are no longer important and only the two auto-relaxation times are needed to describe the motional narrowing limit.

1.12.2.3 Steady-State Overhauser Effect

If the S nucleus is continuously irradiated, *i.e.,* decoupled, while the I spin is detected then

$$\frac{dM_{z_I}}{dt} = -\frac{1}{T_1^{II}}(M_{z_I} - M_{z_I}^{eq}) - \frac{1}{T_1^{IS}}(-M_{z_S}^{eq}) \tag{1.65}$$

Under these conditions $M_{Iz}(t)$ eventually will reach a steady state value of M_{Iz}^{ss} when $\frac{dM_{Iz}}{dt} = 0$. This leads to

$$M_{z_I}^{ss} = M_{Iz}^{eq} + \frac{T_1^{II}}{T_1^{IS}} M_{z_S}^{eq}. \tag{1.66}$$

Rearranging this expression and substituting back into the previous expression we obtain

$$\frac{dM_{z_I}}{dt} = -\frac{1}{T_1^{II}}(M_{z_I} - M_{z_I}^{ss}). \tag{1.67}$$

These last two equations indicate that under continuous irradiation of the S spins, the I magnetization will adjust to a steady state value with a single exponential relaxation time. The enhancement ratio of the steady-state to equilibrium magnetization is given by

$$\epsilon_{NOE} = \frac{M_{z_I}^{ss}}{M_{z_I}^{eq}} = 1 + \eta_{IS}, \tag{1.68}$$

where η_{IS}, given by

$$\eta_{IS} = \frac{\gamma_S}{\gamma_I}\left[\frac{6j(\omega_S + \omega_I) - j(\omega_S - \omega_I)}{j(\omega_S + \omega_I) + 3j(\omega_I) + 6j(\omega_S + \omega_I)}\right], \tag{1.69}$$

is called the steady-state nuclear Overhauser enhancement.

In the motional narrowing regime (small τ_c) the enhancement ratio becomes

$$\epsilon_{NOE} \approx 1 + \frac{\gamma_S}{2\gamma_I}, \tag{1.70}$$

whereas in the slow motion regime ($\omega_0\tau_c > 1$) we find

$$\epsilon_{NOE} \approx \frac{(\gamma_I^2 - \gamma_S^2)(3\gamma_I^2 + 5\gamma_I\gamma_S - 10\gamma_S^2)}{3\gamma_I^4 + \gamma_I^2\gamma_S^2 - 10\gamma_I\gamma_S^3 + 10\gamma_S^4}. \tag{1.71}$$

1.12.3 Quadrupolar Relaxation

In the special case of $I = 1$ a single exponential recovery with time constant T_1 arises from fluctuations of quadrupolar coupling is given by

$$\frac{1}{T_1} = \frac{3}{80}\left(1 + \frac{\eta_q^2}{3}\right)\left(\frac{e^2qQ}{\hbar}\right)^2 [j(\omega_0) + 4\,j(2\omega_0)], \tag{1.72}$$

and

$$\frac{1}{T_2} = \frac{1}{160}\left(1 + \frac{\eta_q^2}{3}\right)\left(\frac{e^2qQ}{\hbar}\right)^2 [9\,j(0) + 15\,j(\omega_0) + 6\,j(2\omega_0)]. \tag{1.73}$$

Here e^2qQ/h is the quadrupole coupling constant and η_q is the asymmetry parameter for the quadrupole coupling.

For nuclei with spin $I > 1$, there will generally be a multi-exponential recovery, and the assumption of a single exponential recovery with time constant T_1 is not valid. In the extreme narrowing case and with the assumption of isotropic molecular tumbling, we obtain a single exponential recovery time for arbitrary spin I, which is given by

$$\frac{1}{T_1} = \frac{1}{T_2} = \frac{3}{40}\frac{2I+3}{I^2(2I-1)}\left(1 + \frac{\eta_q^2}{3}\right)\left(\frac{e^2qQ}{\hbar}\right)^2 \tau_c, \tag{1.74}$$

where τ_c is the molecular reorientation correlation time.

1.12.4 Nuclear Shielding Anisotropy Relaxation

When the electron density around a nucleus is not spherically symmetric the nuclear shielding is a tensor quantity which depends on the orientation local electron density with respect to the external magnetic field. In such a situation the nuclear shielding requires two additional parameters, $\sigma_{||}$ and $\sigma_\perp$ to describe the full tensor. Fluctuations in the nuclear shielding interaction will cause relaxation, described in terms of a single T_1 and T_2 according to

$$\frac{1}{T_1} = \gamma B_0 \left(\sigma_{||} - \sigma_\perp\right) \frac{1}{15} j(\omega_0), \tag{1.75}$$

and

$$\frac{1}{T_2} = \gamma B_0 \left(\sigma_{||} - \sigma_{\perp}\right) \left[\frac{2}{45} j(0) + \frac{1}{30} j(\omega_0)\right]. \tag{1.76}$$

In the extreme narrowing case and with the assumption of isotropic molecular tumbling we obtain

$$\frac{1}{T_1} = \frac{2}{15}\gamma^2 B_0^2 \left(\sigma_{||} - \sigma_{\perp}\right)^2 \tau_c, \tag{1.77}$$

and

$$\frac{1}{T_2} = \frac{7}{45}\gamma^2 B_0^2 \left(\sigma_{||} - \sigma_{\perp}\right)^2 \tau_c. \tag{1.78}$$

1.13 Measuring Chemical Exchange - The Modified Bloch Equations

During a chemical reaction, nuclei can move between chemically nonequivalent environments. Depending on the reaction rate, these processes will manifest themselves differently in the NMR lineshape [1]. In this section, we will examine the simplest example, a single spin 1/2 nucleus experiencing no other spin couplings, and undergoing chemical exchange between two chemically nonequivalent sites, that is,

$$A \underset{k_{-1}}{\overset{k_1}{\rightleftharpoons}} B.$$

In this situation we write the two coupled Bloch equations

$$\frac{d\mathbf{M}_A}{dt} = \gamma(1-\sigma_A)\mathbf{M}_A(t) \times \mathbf{B}(t) - [\mathbf{R}]\{\mathbf{M}_A(t) - \mathbf{M}_{A,eq}\} - k_1\mathbf{M}_A(t) + k_{-1}\mathbf{M}_B(t),$$

$$\frac{d\mathbf{M}_B}{dt} = \gamma(1-\sigma_B)\mathbf{M}_B(t) \times \mathbf{B}(t) - [\mathbf{R}]\{\mathbf{M}_B(t) - \mathbf{M}_{B,eq}\} + k_1\mathbf{M}_A(t) - k_{-1}\mathbf{M}_B(t).$$

We will further simplify our treatment by neglecting the effects of spin relaxation, assuming equal populations of A and B, and that $k = k_1 = k_{-1}$. Solving this set of linear, first-order differential equations, one obtains

$$S(\omega) = \frac{k(\Omega_A - \Omega_B)^2}{(\omega - \Omega_A)^2(\omega - \Omega_B)^2 + 4k^2\Delta\omega^2}, \tag{1.79}$$

where $\Delta\omega = \omega - (\Omega_B + \Omega_A)/2$, as analytical expression for the absorption mode spectrum. In Fig. 1.2 are simulations of the predicted NMR lineshape in a simple two site exchange, based on Eq. (1.79). In the slow exchange limit (low k), the individual resonances for each site are resolved with linewidths, if we include spin-spin relaxation, of $1/T_2 + k$. As the rate of exchange increases the individual lines broaden and coalesce together. In the fast exchange limit the two lines collapse into a single line appearing at the average frequency of the two sites and has a linewidth of $1/T_2 + \frac{1}{2}\Delta\omega^2/k^2$. The decrease in sensitivity in the intermediate regime is more apparent in the spectra on the right of Fig. 1.2, where the lineshapes are normalized to have the same area, a situation that more accurately reflects the experimental sensitivity variations

Given that rate constants often follow the Arrhenius equation

$$k = A\exp(-E_a/RT), \tag{1.80}$$

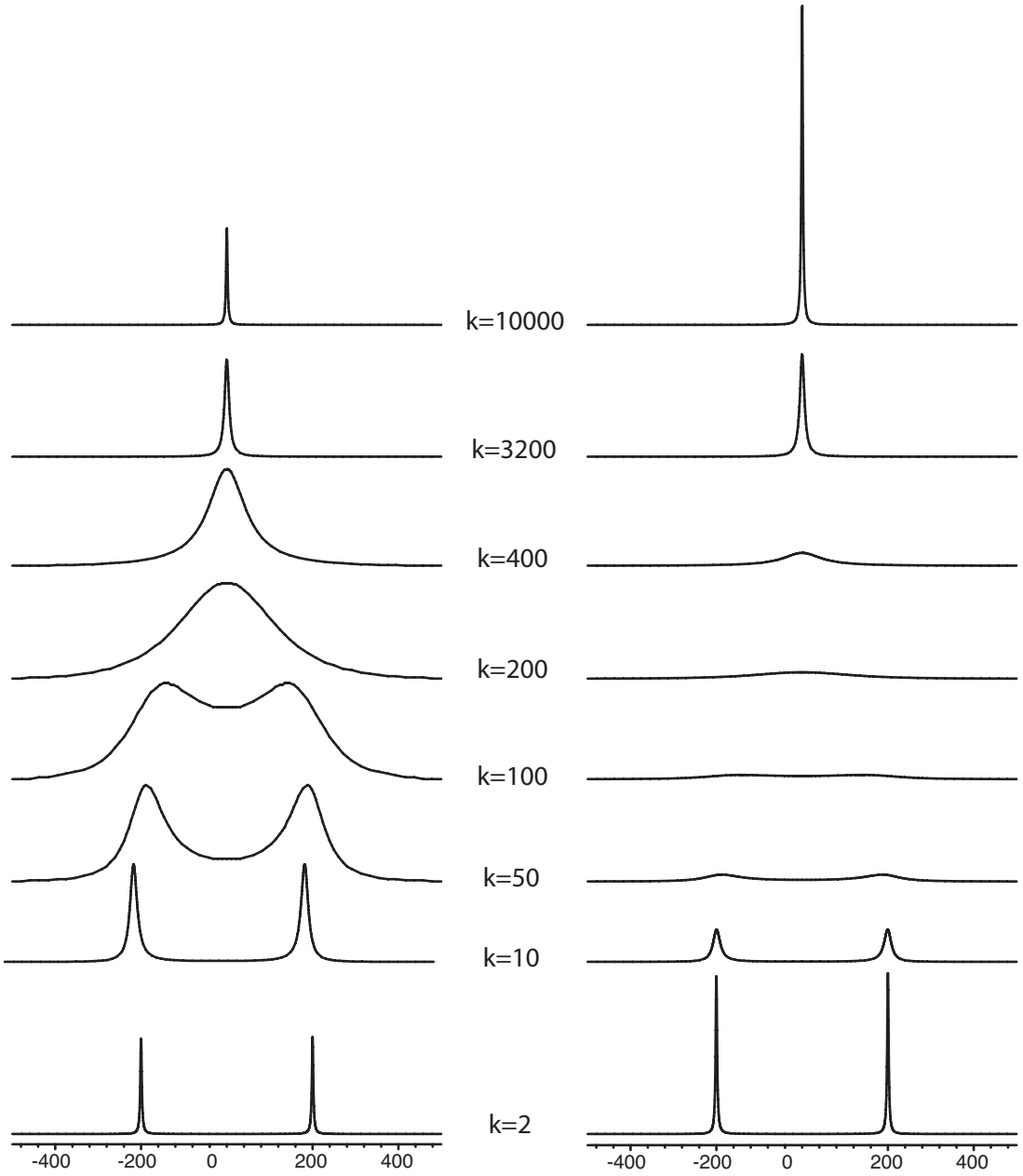

Figure 1.2: NMR lineshape for a two site system ($\Omega_A = -\Omega_B = 200$ Hz) undergoing chemical exchange as a function of rate constant k in s^{-1}. The intensity of the spectra on the left are scaled to the same amplitude to more clearly illustrate the lineshape transformation. The decrease in sensitivity in the intermediate regime is more apparent in the spectra on the right where the lineshapes are normalized to have the same area; a situation that more accurately reflects the experimental sensitivity variations.

P. J. Grandinetti, November 23, 2009

then the evolution of lineshapes with increasing temperature would parallel those in Fig. 1.2 with increasing k. A full lineshape analysis as a function of temperature provides a simple way to measure the activation energy, E_a, for the exchange process.

1.14 Multi-Dimensional NMR

Multi-dimensional NMR originated with Jean Jeener back in the early 1970's and was developed by many others over the last few decades, including Richard Ernst who received the Nobel Prize in Chemistry in 1991.

In two dimensional NMR experiments we define two time domains t_1 and t_2, that are usually divided by some perturbation (typically an rf pulse), and increment both times independent of each other. Now depending on the perturbations you apply and the particulars of the spin system you're exciting, some spins that have one particular frequency during t_1 will have a different frequency during t_2. A 2D spectrum provides us with a map of the correlations between the spin's frequencies in the different time domains.

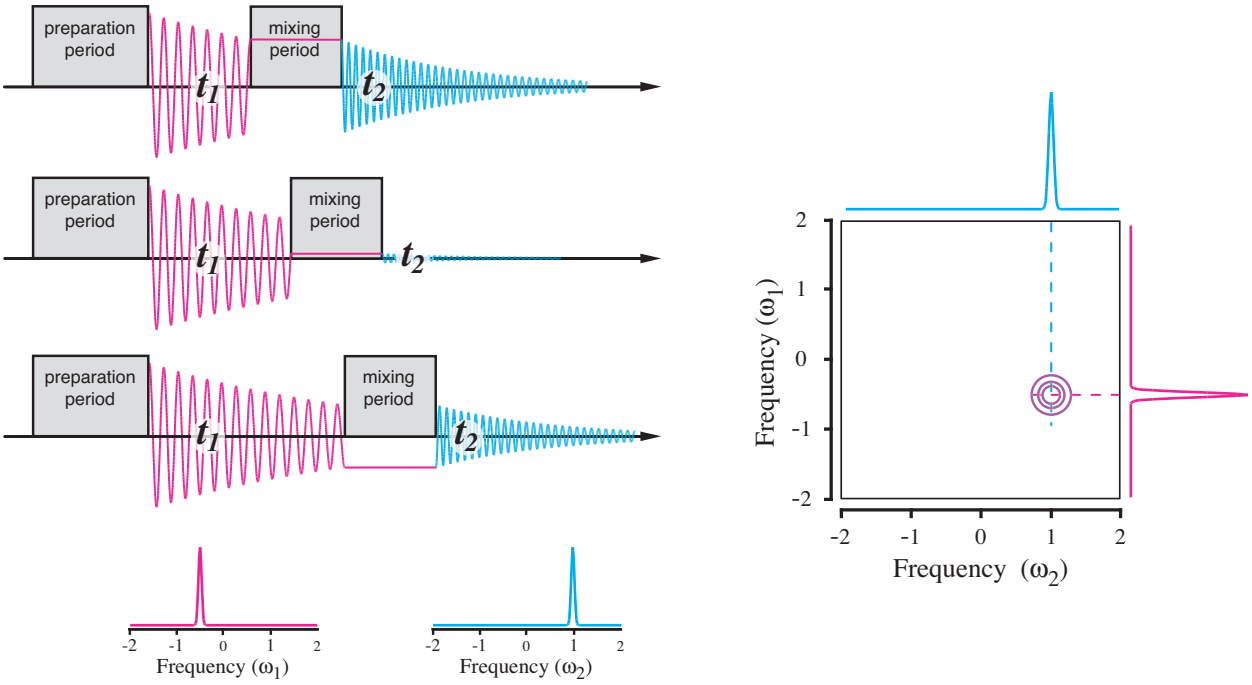

Let's look at a couple examples where such correlations can be exploited to obtain information unavailable in a one-dimensional NMR experiment.

P. J. Grandinetti, November 23, 2009

1.14.1 2D Exchange and 2D NOESY NMR

We saw in section 1.13 how the NMR resonances of two nuclei undergoing chemical exchange will broaden and then coalesce into a single resonance as the rate of exchange increases. The two-dimensional exchange experiment is used to follow chemical exchange processes that occur on a much slower time scale, where the exchange rate has little effect on the lineshapes. The sequence and coherence transfer pathway is shown below.

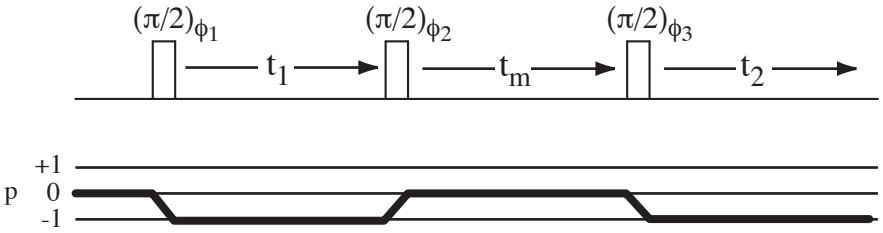

Let's consider this experiment with a system consisting of two chemically distinct but uncoupled spin 1/2 nuclei. We'll label these two sites A and B. One can show that without exchange the signal for these two sites in the experiment above is

$$S(t_1,t_2) = S_A(0,0)e^{i\Omega_A t_1}e^{i\Omega_A t_2}e^{-(t_1+t_2)/T_2^{(A)}} + S_B(0,0)e^{i\Omega_B t_1}e^{i\Omega_B t_2}e^{-(t_1+t_2)/T_2^{(B)}}.$$

If we did a double Fourier transform of this signal with respect to t_1 and t_2, that is,

$$S(\omega_1,\omega_2) = \int_0^\infty \int_0^\infty S(t_1,t_2)e^{i\omega_1 t_1}e^{i\omega_2 t_2}\,dt_1\,dt_2,$$

we would get a two-dimensional spectrum that would look schematically like the one below.

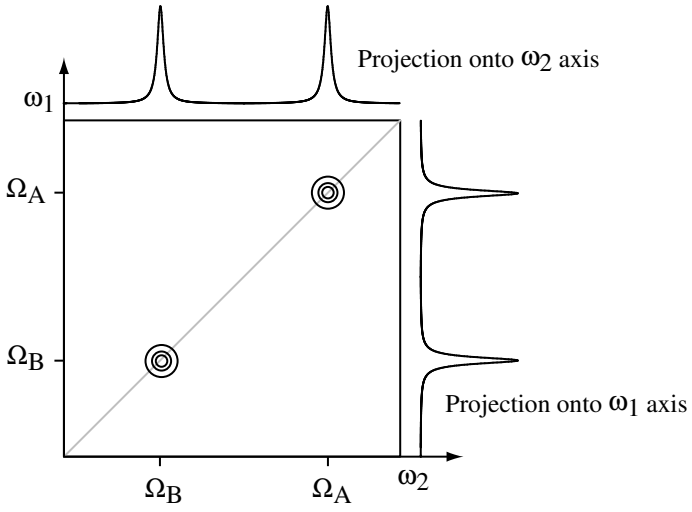

Peaks for the two sites A and B will appear along the diagonal line $\omega_1 = \omega_2$ in the two-dimensional spectrum. On the top and right side of the two-dimensional spectrum are the one-dimensional projections (sums) of the two-dimensional spectrum onto each axis. This two-dimensional spectrum is a plot of how these two one-dimensional spectra (projections) are correlated.

Let's now consider again the two site exchange process where a nucleus is exchanging between sites A and B. When this exchange process is occurring much slower that the individual T_2 times for each site then our two-dimensional spectrum will contain two additional peaks as shown below.

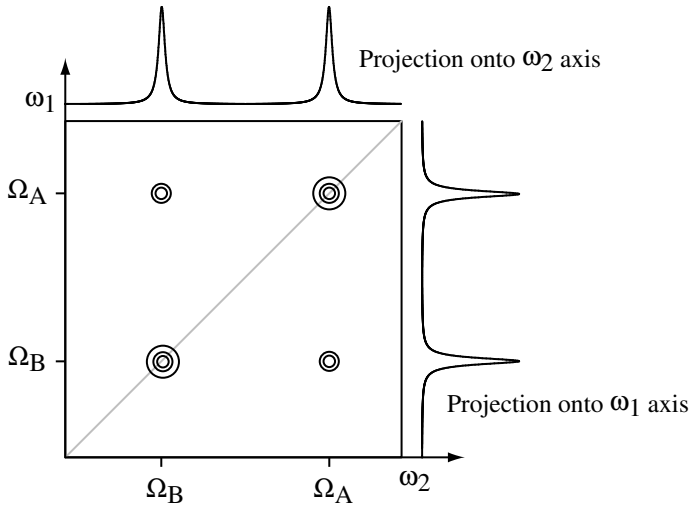

These two new peaks are called cross-correlation peaks and appear on the off-diagonal. For example, the signal at $(\omega_1, \omega_2) = (\Omega_A, \Omega_B)$ corresponds to a nucleus that was in the A environment during t_1 and during t_m exchanged over to the B environment.

Sites along the diagonal are called auto-correlation peaks and correspond to nuclei which were in the same environment for both t_1 and t_2. Clearly when $t_m = 0$ there should be no cross peaks and as t_m is increased, the cross peaks will grow in intensity at the expense of the diagonal peaks. Assuming $k_1 = k_{-1} = k$ and that the sites A and B are equally populated the intensities of the auto-correlation and cross-correlation peaks as a function of mixing time, t_m, are given by

$$a_{AA} = a_{BB} = \frac{1}{2}[1 + \exp(-2kt_m)]\exp(-t_m/T_1), \tag{1.81}$$

$$a_{AB} = a_{BA} = \frac{1}{2}[1 - \exp(-2kt_m)]\exp(-t_m/T_1), \tag{1.82}$$

respectively. From this result one finds that the exchange rate constant can be extracted from the ratio of the cross peak to diagonal peak as a function of t_m, that is,

$$\frac{I_{AA}}{I_{AB}} = \frac{a_{AA}}{a_{AB}} \approx \frac{1 - kt_m}{kt_m}.$$

Below are plots showing typical variations of the auto- and cross-peak intensities as a function of mixing time, when $T_1 = 100$ milliseconds and $k = 30$ sec^{-1}.

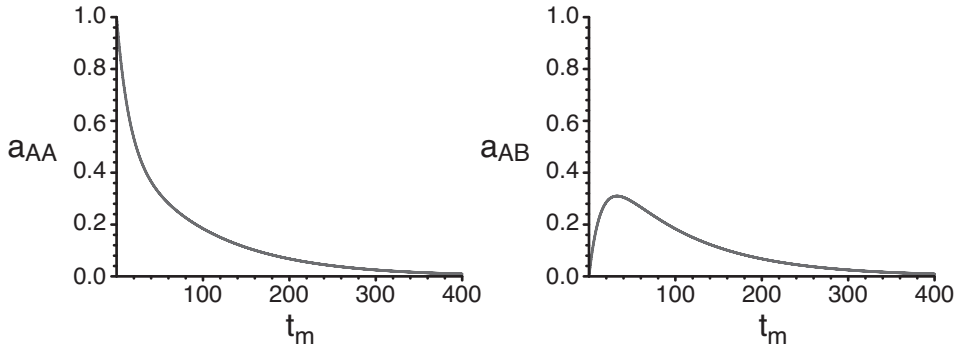

As mentioned in section 1.13, by measuring rate constants, k, as a function of temperature one can obtain the activation energy for the exchange process.

1.14.1.1 Transient nOe's

Not only can chemical exchange generate cross-peak intensity, but relaxation mediated by dipolar coupling between nuclei can also do the same. Recalling our expressions for auto- and cross-relaxation we define auto and cross-relaxation rates for two nuclei of the same isotope (same gyromagnetic ratio and angular momentum) but different resonance frequencies as

$$R_{auto} = 1/T_1^{11} = 1/T_1^{22}, \tag{1.83}$$

and

$$R_{cross} = 1/T_1^{12} = 1/T_1^{21}, \tag{1.84}$$

and rewrite the Solomon equations

$$\begin{aligned} \frac{dM_{z_1}}{dt} &= -R_{auto}(M_{z_1} - M_{z_1}^{eq}) - R_{cross}(M_{z_2} - M_{z_2}^{eq}), \\ \frac{dM_{z_2}}{dt} &= -R_{cross}(M_{z_1} - M_{z_1}^{eq}) - R_{auto}(M_{z_2} - M_{z_2}^{eq}). \end{aligned} \tag{1.85}$$

Solving these equations we find that there will be an exchange of longitudinal magnetization during the mixing time according to

$$M_{1z} \xrightarrow{\tau_m} \cosh(R_{cross}\tau_m)e^{-R_{auto}\tau_m}M_{1z} + \sinh(R_{cross}\tau_m)e^{-R_{auto}\tau_m}M_{2z}, \tag{1.86}$$

$$M_{2z} \xrightarrow{\tau_m} \sinh(R_{cross}\tau_m)e^{-R_{auto}\tau_m}M_{1z} + \cosh(R_{cross}\tau_m)e^{-R_{auto}\tau_m}M_{2z}. \tag{1.87}$$

Thus, we see that cross-peak intensity will be generated by nuclei that cross relax each other. From these equations we can obtain expressions for the auto- and cross-peak amplitudes,

$$a_{auto}(\tau_m) = \cosh(R_{cross}\tau_m)e^{-R_{auto}\tau_m}, \tag{1.88}$$

$$a_{cross}(\tau_m) = \sinh(R_{cross}\tau_m)e^{-R_{auto}\tau_m}. \tag{1.89}$$

At short mixing times these amplitudes can be approximated as

$$a_{auto}(\tau_m) \approx 1, \tag{1.90}$$

$$a_{cross}(\tau_m) \approx R_{cross}\tau_m. \tag{1.91}$$

Recalling our earlier expression for the cross-relaxation rate

$$R_{cross} = \frac{1}{T_1^{IS}} = \frac{I(I+1)}{15}\left(\frac{\mu_0\hbar\gamma_I\gamma_S}{4\pi r^3}\right)^2 \left[j(\omega_I - \omega_S) - 6j(\omega_I + \omega_S)\right], \tag{1.92}$$

we find for the cross-peak amplitude in the motional narrowing limit that

$$a_{cross}(\tau_m) \sim \frac{1}{r^6}. \tag{1.93}$$

1.15 Magnetic Resonance Imaging

Nuclear magnetic resonance can also be used as a tool for imaging samples. By applying a linear magnetic field gradient across the sample,

$$\mathbf{B}(\mathbf{r}) = \mathbf{B}_0 + \mathbf{G} \cdot \mathbf{r},$$

and neglecting relaxation we write the signal in the rotating frame, integrated over the sample volume as

$$S(t) = \int\int\int \rho(\mathbf{r}) e^{i\gamma \mathbf{G}\cdot\mathbf{r}t} d\mathbf{r}, \tag{1.94}$$

where $d\mathbf{r}$ implies integration over the volume of the sample. We could identify this as the time domain signal after applying a $\pi/2$ pulse. On the other hand, if we define the reciprocal space vector $\mathbf{k}$ with

$$\mathbf{k} = \gamma \mathbf{G} t/2\pi, \tag{1.95}$$

we can describe this signal as the nuclear spin density in reciprocal space,

$$S(\mathbf{k}) = \int\int\int \rho(\mathbf{r}) e^{i2\pi \mathbf{k}\cdot\mathbf{r}} d\mathbf{r}, \tag{1.96}$$

Written in this form, the volume integral the signal is recognized as a three-dimensional Fourier transform of the magnetization density in real space. Thus, if we apply a three dimensional inverse Fourier transform to $S(\mathbf{k})$ we obtain the three dimensional real space image of the sample, that is,

$$\rho(\mathbf{r}) = \int\int\int S(\mathbf{k}) e^{-i2\pi \mathbf{k}\cdot\mathbf{r}} d\mathbf{k}. \tag{1.97}$$

There are numerous approaches for doing magnetic resonance imaging. For additional details, the reader is directed to the text by Callaghan listed at the end of the chapter. To illustrate one approach consider the sequence below.

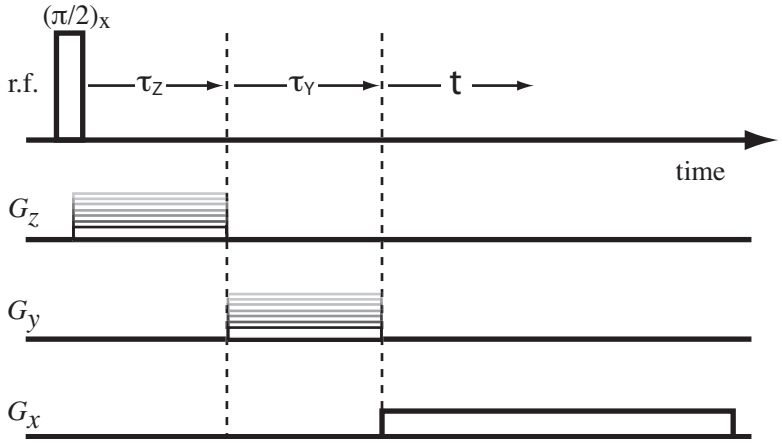

P. J. Grandinetti, November 23, 2009

In this experiment a single $\pi/2$ creates transverse magnetization. Three magnetic field gradients are then applied sequentially along three orthogonal directions. The objective in this experiment is to independently and linearly increase the value of k in all three directions, so that a Fourier transform with respect to all three reciprocal space dimensions leads to a three dimensional real space spin density plot, according to

$$\rho(x,y,z) = \int\int\int S(k_x,k_y,k_z)e^{-i2\pi(k_x x+k_y y+k_z z)}dk_x dk_y dk_z \tag{1.98}$$

From Eq. (1.95) we see that we can vary the size of k through either the size or the duration of the applied field gradient. In the sequence above one increases k_z and k_y by increasing the gradient strengths G_z and G_y with constant durations τ_z and τ_y. Increases in k_x are obtained by acquiring the signal as a function of time with a fixed gradient strength G_x. The medical applications, alone, of magnetic resonance imaging are staggering, and form the basis of a profitable industry. Below is an example of a two-dimensional MRI scan of a human head.

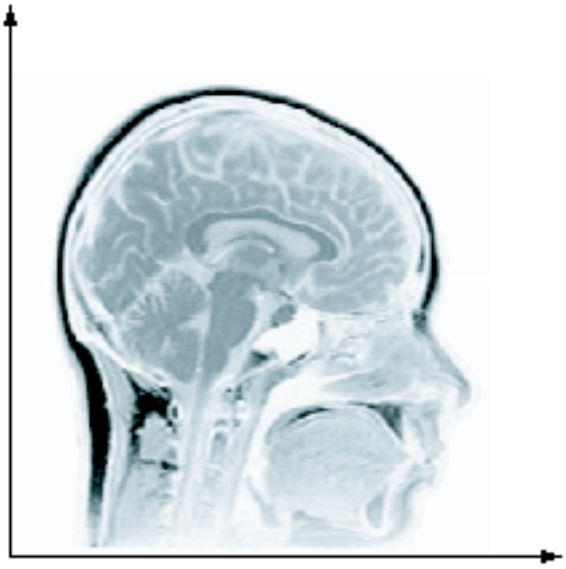

1.16 Summary

Starting with a classical picture of a magnetic top precessing about an external magnetic field, we saw how the precession frequency of that magnetic top could be measured by placing a coil around it, and then measuring the oscillating EMF generated in the coil due to Faraday's Law. We can think of NMR active nuclei as tiny magnetic tops all precessing about the magnetic field with a random distribution of precession phases. The distribution of procession cones, however, was not completely random, and a small excess (ppb) of nuclei were precessing on the $+z$ half of the sphere. Thus, there was a non-zero vector sum of all the nuclear spin magnetic moments along the z-axis.

Using magnetic resonance, we could rotate this net magnetization vector from the z-axis into the x-y plane, and then detect its precession frequency. In the lab frame, the Bloch equations describe the motion of this magnetization vector (including relaxation effects).

$$\frac{d\mathbf{M}}{dt} = \boldsymbol{\omega}(t) \times \mathbf{M}(t) - [\mathbf{R}]\{\mathbf{M}(t) - \mathbf{M}_{eq}\}$$

In the rotating frame, the motion of the magnetization vector becomes simpler (particular during a magnetic resonance rf pulse).

$$\frac{d^*\mathbf{M}}{dt} = \boldsymbol{\omega}_{eff}(t) \times \mathbf{M} - [\mathbf{R}]\{\mathbf{M} - \mathbf{M}_{eq}\}$$

By going into the rotating frame, the precession effects of the large external field can be eliminated, and the small oscillatory fields in the lab frame can appear as small static fields in the rotating frame.

There is a Fourier transform relationship between the signal detected after application of a $\pi/2$ pulse and the NMR spectrum.

For an ensemble of isolated spin 1/2 nuclei we have seen in this chapter that the Bloch equations do a wonderful job of quantitatively describing the NMR experiment. For nuclei with spin greater than 1/2, or for coupled nuclei, however, the Bloch Equations are no longer adequate. The reason for this is that nuclei with $I > 1/2$ have greater degrees of freedom than that of single magnetic dipole moment. It is possible to modify the Bloch Equations to describe additional degrees of freedom, but this motion is just as easily described using the well-established machinery of quantum mechanics. In later chapters, we will look in detail at how quantum mechanics describe the NMR experiment.

Finally, the lineshape of a nucleus undergoing chemical exchange will be affected, in a predictable manner, by the hopping of the atom between two chemically nonequivalent sites. Analysis of this lineshape yields the rate constant for the exchange process.

P. J. Grandinetti, November 23, 2009

Further Reading

- A. Abragam, "Principles of Nuclear Magnetism", Oxford University Press, 1961
- C. P. Slichter, "Principles of Magnetic Resonance", Springer-Verlag, 1980
- R. R. Ernst and G. Bodenhausen and A. Wokaun, "Principles of Nuclear Magnetic Resonance in One and Two Dimensions", Oxford University Press, 1987
- M. H. Levitt, "Spin Dynamics, Basics of Nuclear Magnetic Resonance", Wiley, 2001
- J. I. Kaplan and G. Fraenkel, "NMR of Chemically Exchanging Systems", Academic Press, New York, 1980
- P. T. Callaghan, "Principles of Nuclear Magnetic Resonance Microscopy", 1991

Bibliography

[1] J. I. Kaplan. Chemical exchange effects on spectra. In David M. Grant and Robin K. Harris, editors, *Encyclopedia of Nuclear Magnetic Resonance*, pages 1247–1256. John Wiley & Sons, 1995.

[2] M. Bloom and M. A. LeGros. Direct detection of two-quantum coherence. *Can. J. Phys.*, 64:1522–1528, 1986.

[3] M.-Y. Liao and G. S. Harbison. The nuclear hexadecapole interaction of iodine-127 in cadmium iodide measured using zero-field two dimensional nuclear magnetic resonance. *J. Chem. Phys.*, 100(3):1895–1901, 1994.

[4] D. W. McCall, D. C. Douglass, and E. W. Anderson. Self-diffusion studies by means of nuclear magnetic resonance spin-echo techniques. *Ber. Bunsenges. Physik. Chem.*, 67:336–340, 1963.

[5] P. Stilbs. Fourier transform pulsed-gradient spin-echo studies of molecular diffusion. *Prog. Nucl. Magn. Reson. Spectros.*, 19:1–45, 1987.

[6] E. O. Stejskal and J. E. Tanner. Spin diffusion measurements: Spin echoes in the presence of a time-dependent field gradient. *J. Chem. Phys.*, 42(1):288–292, 1965.